A dynamic compositional equilibrium governs mRNA recognition by eIF3

Nicholas A. Ide[1,*], Riley C. Gentry[1,*], Margaret A. Rudbach[3], Kyungyoon Yoo[3,5], Paloma Kai Velez[3], Victoria M. Comunale[2], Erik W. Hartwick[2,6], Colin D. Kinz-Thompson[2,7], Ruben L. Gonzalez Jr.[2,†], and Colin Echeverría Aitken[3,4,†]

[1] *Department of Biological Sciences, Columbia University, New York, NY, USA*
[2] *Department of Chemistry, Columbia University, New York, NY, USA*
[3] *Biochemistry Program, Vassar College, Poughkeepsie, NY, USA*
[4] *Biology Department, Vassar College, Poughkeepsie, NY, USA*
[5] *Current Address: Renaissance School of Medicine, Stony Brook University, Stony Brook, NY, USA*
[6] *Current Address: Biochemistry Krios Electron Microscopy Facility, Department of Biochemistry, University of Colorado Boulder, Boulder, CO, USA*
[7] *Current Address: Department of Chemistry, Rutgers University-Newark, Newark, NJ, USA*

* These authors contributed equally to this work
† To whom correspondence may be addressed: Ruben L. Gonzalez, Jr, Department of Chemistry, Columbia University, 3000 Broadway, New York, NY 10027, Tel: (212) 854-1096, Email: rlg2118@columbia.edu and Colin Echeverría Aitken, Department of Biology, Vassar College, Olmsted Hall of Biological Sciences, Box 731 Poughkeepsie, NY, 12604, Tel: (845) 437-7430, Email: caitken@vassar.edu

SUMMARY
Eukaryotic translation initiation factor (eIF) 3 is a multi-subunit protein complex that binds both ribosomes and messenger RNAs (mRNAs) to drive a diverse set of mechanistic steps during translation of an mRNA into the protein it encodes. And yet, a unifying framework explaining how eIF3 performs these numerous activities is lacking. Using single-molecule light scattering microscopy, we demonstrate that *Saccharomyces cerevisiae* eIF3 is in dynamic exchange between the full complex, subcomplexes, and subunits. By extending our microscopy approach to an *in vitro* reconstituted eIF3 and complementing it with biochemical assays, we define the subspecies comprising this dynamic compositional equilibrium and show that mRNA binding by eIF3 is not driven by the full complex but instead by the eIF3a subunit within eIF3a-containing subcomplexes. Our findings provide a mechanistic model for the role of eIF3 in mRNA recruitment and establish a mechanistic framework for explaining and investigating the other activities of eIF3.

KEYWORDS
Translation, translation initiation, eIF3, mRNA, mRNA recruitment, ribosome, translational regulation, single-molecule, mass photometry, biophysics, biochemistry

INTRODUCTION

Initiation of translation at the start codon of a messenger RNA (mRNA) sets the reading frame for protein synthesis and is the most regulated stage of translation[1-5]. In eukaryotes, initiation is distinguished by an mRNA recruitment step during which a ribosomal pre-initiation complex (PIC) attaches near the 7-methylguanosine 'cap'-containing 5' end of the mRNA and then scans to locate the start codon. mRNA recruitment determines how a diverse set of mRNAs compete for the translation machinery.

Eukaryotic translation initiation factor (eIF) 3 is a multi-subunit protein complex composed of 5-12 subunits, depending on the species, that is required for mRNA recruitment to the 43S PIC during initiation[6-9]. eIF3 has more recently been implicated in mediating events during translation elongation[10] and termination[11], and has emerged as a player in translational regulation at multiple stages and by various proposed mechanisms[12-18]. And yet, how the role of eIF3 in mRNA recruitment is related to these emerging regulatory roles and their underlying mechanisms remains a mystery.

Each of these proposed roles suggests eIF3 interacts directly or indirectly with mRNA. During initiation, eIF3 binds the PIC[2,6] and its presence near the mRNA-entry channel of the ribosomal small, or 40S, subunit appears to facilitate loading of the mRNA onto the PIC and subsequent scanning of the PIC along the mRNA to locate the start codon[19-21]. At the mRNA-exit channel of the PIC, eIF3 makes critical contributions to stabilizing the binding of mRNA to the PIC[22]. However, the mechanistic origin of these effects remains unclear. Multiple lines of evidence also suggest eIF3 remains bound to post-initiation, ribosomal elongation complexes engaged in translating specific mRNAs to regulate their expression by an unknown mechanism[10,23] and that eIF3 can mediate sequence-specific re-initiation events[24]. Finally, multiple studies have reported that eIF3 binds specific mRNAs directly or indirectly and may thus dictate their translational fates[12,13,25]. Nonetheless, it remains unclear whether these interactions are mediated by the full eIF3 complex containing all of its component subunits (hereafter referred to as the full eIF3 complex) or by smaller multi-subunit eIF3 subcomplexes or even individual, complex-free, eIF3 subunits. In fact, some evidence suggests that distinct eIF3 subcomplexes associate with specific mRNA pools to differentially control their translation[26]. And yet, a mechanism for this compositional heterogeneity and how it might underlie these differential outcomes remains elusive.

Whether various molecular species are responsible for the different functions of eIF3 and, if so, which species drives which function remain unanswered questions in the field. These questions are in line with a growing body of evidence showing that multi-subunit protein complexes, which are widespread in biology and play essential roles in gene expression and beyond[27-29], are not indefinitely stable and compositionally uniform. Instead, they are metastable and compositionally heterogeneous[30,31]. In the yeast *Saccharomyces cerevisiae*, eIF3 is composed of five essential subunits that are conserved throughout eukaryotes and thought to represent a functional core complex[6] that in humans has expanded to 12 subunits[9]. The possibility that eIF3 behaves not as a single molecular species but instead as a mixture of distinct subspecies might explain the myriad roles attributed to eIF3 as well as its ability to mediate distinct but specific translational fates across various mRNAs. Nonetheless, such a model remains unexplored.

To directly test this hypothesis, we have combined a novel single-molecule light scattering microscopy technique and a battery of ensemble biophysical and biochemical assays to investigate the compositional integrity and biochemical functions of natively purified and *in vitro* reconstituted *S. cerevisiae* eIF3. Leveraging our ability to control the composition of reconstituted eIF3, we conclusively demonstrate that, rather than functioning as a single, highly stable, and uniform entity, the full eIF3 complex is in a dynamic equilibrium with its constituent components. Exploiting our capacity to characterize this dynamic equilibrium and detect the binding of individual eIF3 subspecies to mRNA at the single-molecule level, we interrogate the contributions

that individual eIF3 subcomplexes and subunits make to mRNA binding by eIF3. Our findings provide a mechanistic framework for understanding how the binding of mRNA by specific eIF3 subspecies contributes to the mechanism of mRNA recruitment by the PIC. More broadly, the framework we have uncovered provides a clear rationale for how eIF3 can execute the many and diverse roles that have been attributed to it, particularly in higher eukaryotes, where the more complex subunit composition of eIF3 could enable a more multiplexed array of subspecies with distinct biochemical functions.

RESULTS

A dynamic equilibrium governs eIF3 composition

In vivo genetic and biochemical studies of eIF3 suggest that individual eIF3 subcomplexes and subunits might play functional roles in cells[26,32-35]. Contrasting with this possibility, analyses of data from *in vitro* biochemical studies of eIF3 have universally made the simplifying assumption that eIF3 functions as a single, stable complex containing the full set of eIF3 subunits (*i.e.*, the full eIF3 complex)[22,36]. Consistent with this view, size-exclusion chromatography of eIF3 runs as a single peak, albeit typically exhibiting some broadness, shouldering, and/or splitting[37-40] (Figure S1A). Motivated by these contrasting perspectives, we set out to characterize the compositional stability of native eIF3 purified from *S. cerevisiae*. To this end, we employed a single-molecule interferometric scattering (iSCAT) microscopy technique that detects the adsorption of an individual particle onto the borosilicate glass surface of a microscopy sample well (Refeyn, Inc.). iSCAT microscopy measures the interference between a reference laser light field that is reflected off of the surface of the well and the Rayleigh scattering of this light field that occurs when individual, subwavelength-sized particles adsorb to the surface. iSCAT is a wide-field microscopy technique in which the adsorption of hundreds to thousands of individual particles to the surface of the well can be spatially separated and imaged using a complementary metal-oxide semiconductor (CMOS) camera[41]. Although it is possible that different particles exhibit differential adsorption to the surface, the mass distribution of particles adsorbed to the surface has been shown to closely approximate the mass distribution of particles in solution (*i.e.*, the 'solution mass distribution')[42]. Because the amount of scattering increases as the size of the particle increases, the iSCAT microscope allows the particles present in a complex mixture to be distinguished based upon their molecular mass. The conventional output of this mass photometry technique is a one-dimensional histogram in which the number of peaks corresponds to the number of species that can be resolved[43,42].

To reveal the solution composition of the full eIF3 complex, we began by characterizing a 30 nM sample of natively purified eIF3, which we have previously shown is biochemically active[44]. If a 30 nM sample of eIF3 contained a single, highly stable, and uniformly composed full eIF3 complex, we would expect to observe a single major species with a molecular mass of ~360 kDa. In contrast with this expectation, we observe at least four distinct species (Figure 1A and Table S1). While one of these species does appear at ~360 kDa, reflective of the full eIF3 complex (Figure 1A), there are three additional peaks present at lower molecular masses, which likely reflect the presence of either individual eIF3 subunits and/or subcomplexes. Because eIF3 subunits make numerous contacts with each other[6,40] there are many possible subcomplexes that may form. Therefore, to conservatively distinguish these subcomplexes from the subunits and full complex, we used threshold cutoffs based on the expected molecular masses of individual eIF3 subunits, subcomplexes, and the full complex determined from the protein sequences of each subunit (Figures 1C, 1D, S2 and Table S1). The largest individual subunit is eIF3a, with a molecular mass of 111.5 kDa. Therefore, 'subunits' were defined as any species with molecular masses between 0 and 120 kDa. The full eIF3 complex has a molecular mass of 360.5 kDa. Therefore, we defined the 'full complex' as any species with a molecular mass between 320 and 450 kDa. Following these definitions, we defined 'subcomplexes' as any species with a molecular mass between 120 and 320 kDa, which fits well with the expected molecular masses for various

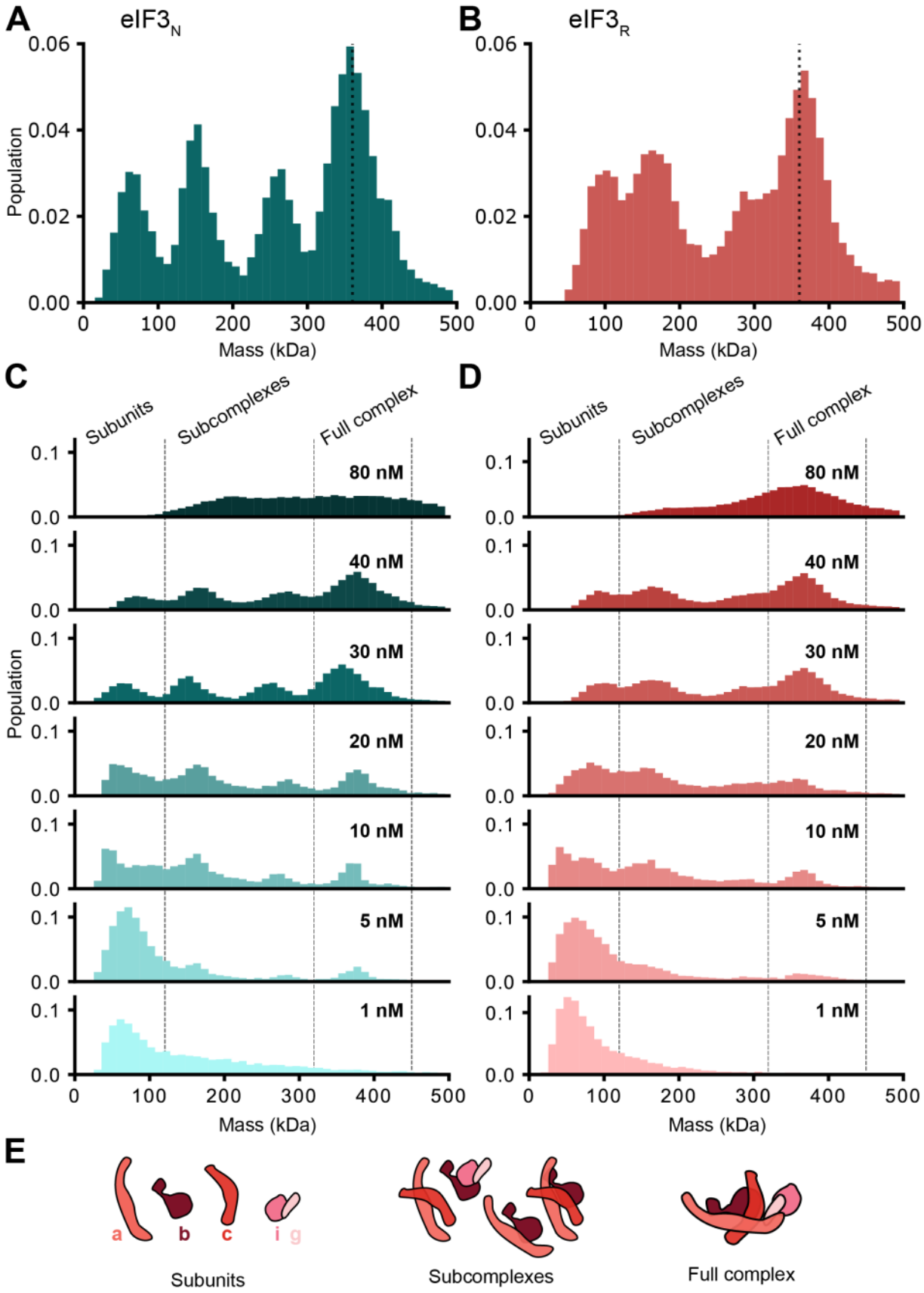
A
eIF3N
B
eIF3R
Population
Mass (kDa)
C
D
Subunits
Subcomplexes
Full complex
80 nM
40 nM
30 nM
20 nM
10 nM
5 nM
1 nM
E
a
b
c
i
g
Subunits
Subcomplexes
Full complex

Figure 1. eIF3 exists as a dynamic equilibrium between subunits, subcomplexes, and the full complex. (A) *Mass distribution histograms of eIF3$_N$ at 30 nM obtained using mass photometry. The dotted black line indicates the expected ~360 kDa molecular mass for the full eIF3 complex.* ***(B)*** *The equivalent plot as shown in (A) for eIF3$_R$.* ***(C)*** *Mass distribution histograms of eIF3$_N$ at various concentrations. Dashed grey lines indicate the threshold cutoffs defining 'subunits' (0-120 kDa), 'subcomplexes' (120-320 kDa), and the 'full complex' (320-450 kDa).* ***(D)*** *The equivalent plot as shown in (C) for eIF3$_R$.* ***(E)*** *Simplified cartoon models denoting the eIF3 subunits, representative subcomplexes, and full complex.*

eIF3 subcomplexes (Table S1). We validated these thresholds by mapping them onto the mass distributions we obtained from mass photometry experiments performed using individual eIF3 subunits and subcomplexes, confirming that the thresholds distinguish between these species (Figure S3). Using these thresholds for eIF3 at 30 nM, the population of subunits is 14.3 ± 2.6 %, the population of subcomplexes is 33.5 ± 2.7 %, and the population of the full complex is 34.7 ± 1.4%. We note that the lower mass resolution limit of mass photometry is ~60 kDa[41], such that peaks below ~60 kDa could represent multiple species with molecular masses at or lower than ~60 kDa. These results reveal that the composition of eIF3 is governed by an equilibrium involving the full complex and its constituent subcomplexes and subunits.

The equilibria that typically control multi-subunit biomolecular complexes are dynamic, such that individual subunits exchange between a full complex, subcomplexes, and/or complex-free subunits over time. To assess whether the eIF3 compositional equilibrium is dynamic on the scale of seconds, we used mass photometry to characterize the compositional equilibrium of an 80 nM eIF3 sample that we then serially diluted down to 1 nM while re-characterizing the equilibrium at each concentration (Figures 1A and S2C). We note here that, due to the high number of adsorption events at 80 nM, the spatial resolution between the full complex, subcomplexes, and subunits in mass photometry can become compromised[41], potentially resulting in under-sampling of low-molecular-mass species. Nonetheless, consistent with expectations for a dynamic compositional equilibrium, the mass distribution histograms at the highest eIF3 concentrations are largely composed of higher-order subcomplexes and the full complex, but transition to be largely composed of subunits at the lowest eIF3 concentrations (Figure S2C). Importantly, systematically increasing or decreasing by 20 kDa the molecular weight thresholds we set to distinguish subcomplexes from subunits and the full complex does not change these overall trends (Figure S2C), demonstrating that this analysis method is robust and insensitive to the selection of particular threshold values.

Identification and characterization of eIF3 species using an *in vitro* reconstituted eIF3

To assign the observed peaks to specific subcomplexes or subunits and to explore the potential role of this equilibrium in regulating eIF3 function, we sought to modulate the presence and concentrations of the individual subunits. Because all five *S. cerevisiae* subunits are essential, it is not possible to natively purify eIF3 variants from strains that lack one or more subunits or contain other lethal mutations. To overcome this challenge, we optimized a system for *in vitro* reconstituting eIF3 from *S. cerevisiae* subunits that are recombinantly expressed in *Escherichia coli*[39,40] (STAR*Methods, Figure S1B). Briefly, we individually purified recombinant eIF3a, eIF3b, and eIF3c, as well as an eIF3i-eIF3g fusion that we subsequently separated *via* proteolytic cleavage during purification. Combining these purified subunits in near stoichiometric amounts yields an *S. cerevisiae* reconstituted eIF3 (eIF3$_R$) that, upon size-exclusion chromatography, runs as a single peak similar to that observed for *S. cerevisiae* native eIF3 (eIF3$_N$) (Figure S1A).

Using mass photometry, we assessed whether eIF3$_R$ exhibits a dynamic compositional equilibrium comparable to that which we observed for eIF3$_N$ (Figure 1B). Using the same threshold values defined above (Figure 1D), 30 nM eIF3$_R$ was composed of 12.9 ± 2.2 % subunits, 41.2 ± 1.4 % subcomplexes, and 35.7 ± 2.5 % full complex, populations of eIF3 species that are similar to those observed for 30 nM eIF3$_N$ (Figures S2C and S2D). Analogous to our studies of

the $eIF3_N$ compositional equilibrium, we next performed mass photometry measurements of an 80 nM $eIF3_R$ sample and of serial dilutions of this sample down to 1 nM $eIF3_R$. In agreement with the dynamic nature observed for the $eIF3_N$ compositional equilibrium, the 80 nM $eIF3_R$ sample is primarily composed of the full complex, and dilution of this sample shifts the $eIF3_R$ compositional equilibrium away from the full complex, initially populating the subcomplexes at intermediate concentrations, and ultimately populating the individual subunits at the lower concentrations (Figures 1D and S2D). Again, shifting the threshold value selection up or down by 20 kDa did not significantly alter the population distributions (Figure S2D). Collectively, our results using $eIF3_N$ and $eIF3_R$ demonstrate that the composition of eIF3 is governed by a dynamic equilibrium in which the full complex is in dynamic exchange with its constituent subcomplexes and subunits.

In an effort to identify which eIF3 subspecies underlie the peaks observed within the subunit, subcomplex, and full complex mass ranges defined by our molecular mass thresholds, we performed mass photometry experiments on 30 nM samples of the purified individual $eIF3_R$ subunits (Figure S3A) and combinations of $eIF3_R$ subunits selected based on the expectation they would form relatively stable subcomplexes, as reported in previous genetic[45,46], biochemical[32,47], and 48S PIC structural studies[8,20,21,46,48-50] (Figure S3B). To determine the center of each peak in each experiment, the mass distribution histograms were fit to a mixture of Gaussian functions (STAR*Methods, Figures S2A and S2B, and Table S1). Using this method for the 30 nM $eIF3_R$ sample, we identified species centered at 367, 275, 170, and 97 kDa, a result that closely matches

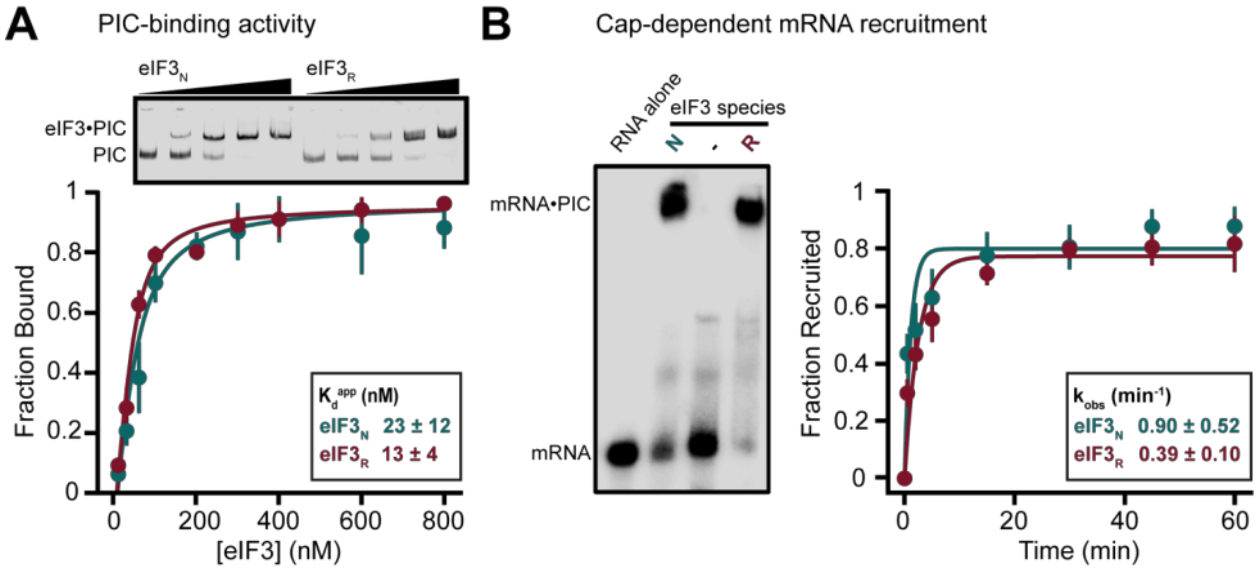

Figure 2. $eIF3_R$ is biochemically active. (A) *Electrophoretic mobility shift assay (EMSA) comparing $eIF3_N$ and $eIF3_R$ binding to the PIC. An example gel is shown (top) alongside the quantitation across three replicates (bottom), including the apparent binding affinities (K_d^{app}).* ***(B)*** *EMSA comparing the ability of $eIF3_N$ and $eIF3_R$ to stimulate recruitment of capped rpl41a mRNA. An example gel is shown (left) alongside the quantitation across three replicates (right), including the observed rate constants (k_{obs}).*

that for the 30 nM $eIF3_N$ sample (Table S1). By comparing these peak centers to those obtained from the mass distribution histograms of the individual $eIF3_R$ subunits and selected combinations of $eIF3_R$ subunits we were able to assign the species centered at 367 kDa to the full complex; the species centered at 275 kDa to the eIF3abig and/or eIF3abc subcomplexes; the species centered at 170 kDa to the eIF3big, eIF3ab, and/or eIF3ac subcomplexes; and the species centered at 97 kDa to the eIF3ig subcomplex and/or to the eIF3a , eIF3b, and/or eIF3c subunits (Figure S3 and Table S1). These results demonstrate that the subcomplexes predicted to form by previous

genetic[45,46], biochemical[32,47], and 48S PIC structural studies[8,20,21,46,48-50] do indeed form and, more importantly, are present within the mixture of species that constitute the eIF3 dynamic compositional equilibrium.

eIF3$_R$ recapitulates the biochemical activities of eIF3$_N$

Before investigating the role that the dynamic eIF3 compositional equilibrium might play in regulating eIF3 function, we sought to characterize the biochemical activity of eIF3$_R$ and compare it to that of eIF3$_N$. While there have been three previous reports of recombinantly reconstituted eIF3, none of these have been validated using *in vitro* assays testing the various functions of eIF3[35,39,40]. To this end, we used two established eIF3 activity assays. The first of these is an assay that monitors eIF3 binding to the PIC[22,51]. Using a previously described[22,51,52], uncapped and unstructured, 50-nucleotide model mRNA containing an AUG start codon at nucleotide positions 23-25 and a fluorescein label at the 3' end, we employed a previously reported *S. cerevisiae in vitro* reconstituted translation initiation system[37,38] to assemble PICs (STAR*Methods). Briefly, we combined mRNA and 40S subunits with saturating amounts of a ternary complex composed of eIF2, guanosine triphosphate (GTP), and initiator transfer RNA (eIF2(GTP)•tRNA$_i$), eIF1, and eIF1A to form PICs under conditions previously reported to yield start-codon-dependent formation of PICs in the absence of the eIF4 factors[22,36]. We then incubated these PICs with varying concentrations of either eIF3$_R$ or eIF3$_N$ and used native gel electrophoresis to separate free mRNA, eIF3-free PICs, and eIF3-bound PICs (Figure 2A). Consistent with a previous study that reported a mean apparent equilibrium dissociation constant (K_d^{app}) of 30 nM for eIF3$_N$ binding to the PIC[22], we observe a mean K_d^{app} of 23 nM for eIF3$_N$ binding to the PIC (Figure 2A, Teal). More importantly, we observe a mean K_d^{app} of 14 nM for eIF3$_R$ binding to PICs (Figure 2A, Burgundy), demonstrating that our eIF3$_R$ binds the PIC nearly identically to eIF3$_N$.

The second activity assay leverages the fact that eIF3 is required for *in vitro* recruitment of capped mRNAs into PICs[22,36,44,52,53]. Using this mRNA recruitment assay, we compared the abilities of eIF3$_R$ and eIF3$_N$ to recruit a capped mRNA encoding the *S. cerevisiae rpl41a* gene into PICs as a function of time. The rpl41a mRNA has previously been used as a representative natural mRNA in numerous *in vitro* and *in vivo* biochemical studies[22,36,52,54]. Briefly, we prepared a mixture containing PICs (eIF1, eIF1A, and ternary complex in concentrations high enough over the 40S subunit to saturate the mRNA recruitment activity and, when included, the specified concentration of either eIF3$_R$ or eIF3$_N$), the eIF4 factors (eIF4G, eIF4E, eIF4A, and eIF4B at concentrations high enough over the mRNA to saturate the mRNA recruitment activity), and ATP (STAR*Methods). To begin each reaction, we added a sub-stoichiometric amount of the rpl41a mRNA prepared with a ^{32}P-labeled cap to the mixture, incubated for a variable amount of time, and used native gel electrophoresis to separate free mRNA from mRNA recruited to PICs. Under conditions in which they are saturating over the PIC, both eIF3$_R$ and eIF3$_N$ stimulate mRNA recruitment similarly across timepoints ranging from 30 seconds to 60 minutes (Figure 2B). Under conditions in which they are sub-saturating to saturating over the PIC, both eIF3$_R$ and eIF3$_N$ stimulate > 70 % mRNA recruitment. Although the mRNA recruitment efficiency of eIF3$_R$ and eIF3$_N$ are within error at each concentration tested (Figure S4), the modest differences we observe could derive from contamination of the eIF3$_N$ preparation with additional proteins, which is routinely observed in preparations of eIF3$_N$[20,38]. Alternatively, or in addition, these slight activity differences might derive from previously observed variations in the mRNA recruitment activities of different preparations of eIF3[38], from the presence of post-translational modifications in eIF3$_N$ that are lacking in our eIF3$_R$, or from subtle variations in the subunit stoichiometry of eIF3$_N$ (as compared to eIF3$_R$). Regardless, the collective results of these assays demonstrate that eIF3$_R$ recapitulates the known *in vitro* biochemical functions of eIF3$_N$.

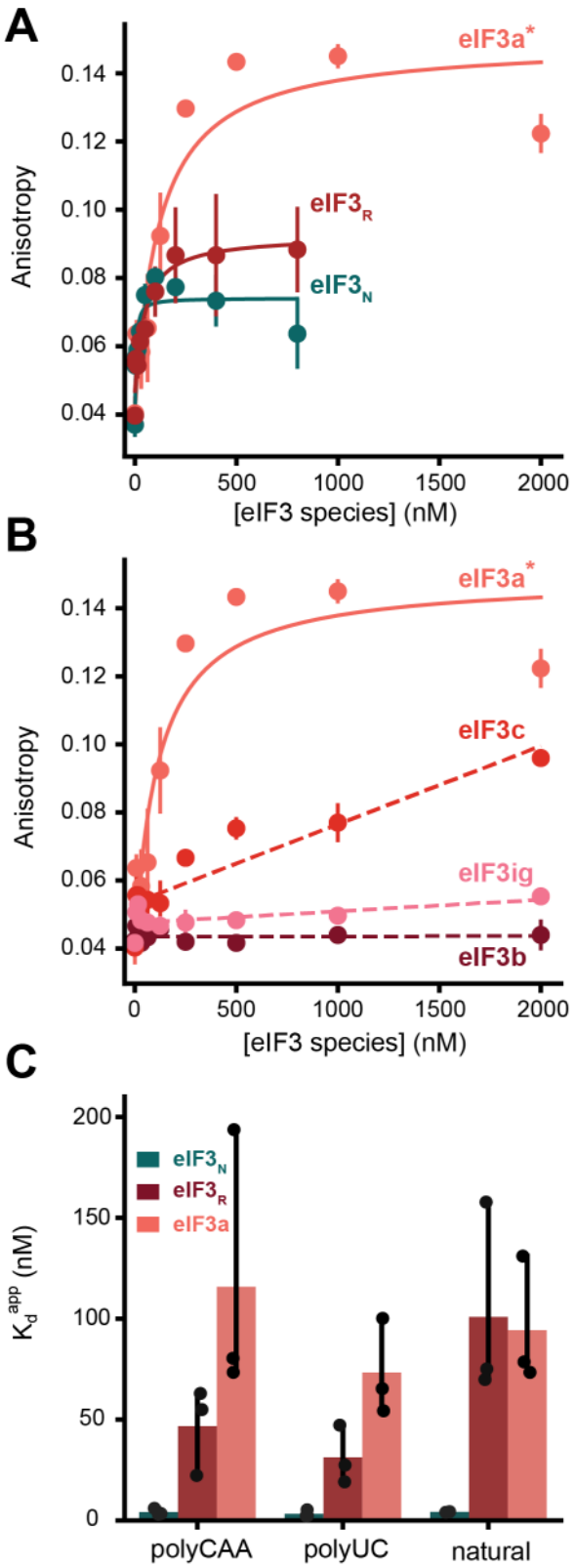

Figure 3. eIF3a is the only subunit that binds mRNA with high affinity. (A) *Fluorescence-anisotropy experiments comparing eIF3$_N$, eIF3$_R$, and eIF3a* binding to an mRNA.* ***(B)*** *Fluorescence-anisotropy*

experiments comparing eIF3a, eIF3b, eIF3c, and a co-purified eIF3i-eIF3g binding to an mRNA. *The binding curve for eIF3a shown in panels (A) and (B) are the same data shown for comparison.* ***(C)*** *Bar graph of the apparent binding affinities measured for three sequence-distinct mRNAs to eIF3$_N$, eIF3$_R$, and eIF3a.*

eIF3a is the only free eIF3 subunit that binds mRNA with high affinity

One of the most recently described functions of eIF3, an activity that is typically ascribed to the full complex, is its apparent ability to directly interact with specific mRNAs in cells[12,13,16,25]. This is an exciting development in that it suggests that direct interactions between eIF3 and specific mRNAs could drive initiation of such mRNAs[13,14,55]. Consistent with this model, previous *in vitro* mRNA binding assays have shown that eIF3 can bind mRNA with a K_d^{app} of 30 nM[36]. Complementing this, previous *in vivo* and *in vitro* biochemical studies have identified several eIF3 subunits from *S. cerevisiae* or higher eukaryotes that copurify or crosslink with either endogenous or model mRNAs[13-18,25,36,56-60]. These latter results motivated us to ask whether individual eIF3$_R$ subcomplexes and/or subunits exhibit high-affinity mRNA binding and, if so, whether the dynamic eIF3 compositional equilibrium might regulate the ability of eIF3 to bind mRNA.

We began by testing whether eIF3$_R$ binds to mRNA and compared it to our own experiments with, and what has been previously reported for, eIF3$_N$[36]. Using the same uncapped, 50-nucleotide, 3'-fluorescein-labeled model mRNA that we used in the PIC binding assays described above, we measured changes in the fluorescence anisotropy of mRNA upon titration with either eIF3$_R$ or eIF3$_N$ (Figure 3A). Fitting plots of fluorescence anisotropy as a function of eIF3 concentration to a model assuming that eIF3 binds as a single species to a single site provides mean K_d^{app} values of 5 nM and 45 nM for eIF3$_N$ and eIF3$_R$, respectively (Figure 3A), in excellent agreement with the mean K_d^{app} of 30 nM that has been previously reported for eIF3[36]. The differences we observe in the fluorescence anisotropy as a function of eIF3 concentration for eIF3$_R$ and eIF3$_N$ are likely due to differences in the stoichiometries of the individual subunits within eIF3$_N$ versus those within the more stoichiometrically uniform eIF3$_R$; this interpretation is supported by our experiments showing that distinct eIF3 species bind to mRNA with significantly different affinities, as described below. Nonetheless, these results demonstrate that eIF3$_R$ recapitulates the mRNA binding activity of eIF3$_N$.

We next leveraged our eIF3$_R$ system to test whether and to what extent individual eIF3 subunits can directly interact with mRNAs. To accomplish this, we adapted the fluorescence anisotropy-based mRNA binding assay described above to measure the change in fluorescence anisotropy of the mRNA upon titration with individual eIF3 subunits (Figures 3B, S5B, and S5D). Because we co-purify eIF3i and eIF3g and they form a high-affinity bimolecular complex that is not easily separated[39,40], we titrated these together. Surprisingly, despite the fact that both eIF3b and eIF3g contain RNA recognition motifs[57,58,60], plots of fluorescence anisotropy as a function of eIF3 subunit concentration reveal that neither eIF3b nor eIF3ig show an appreciable level of mRNA binding, even at the highest protein concentrations tested (2 μM). Moreover, eIF3c exhibits only modest affinity for mRNA, with a K_d^{app} of > 600 nM (Figure S5B and Table S2). In stark contrast, eIF3a exhibits significant mRNA binding activity, yielding a mean K_d^{app} of 116 nM that could potentially account for a significant fraction of the mRNA binding affinity we observed when titrating mRNA with eIF3$_N$ or eIF3$_R$ (mean K_d^{app} values of 5 and 45 nM, respectively). Notably, the relatively high mRNA binding affinities we observed here for eIF3$_N$, eIF3$_R$, and eIF3a all required an mRNA length of at least 45 nucleotides (Table S2 and Source Data). To test the effect of the model mRNA sequence on eIF3 binding, we tested a different model mRNA with a distinct repetitive sequence[37] (Figures S5A and S5B) as well as a model mRNA containing the first 51 nucleotides of the native rpl41a sequence (Figures S5C and S5D). Neither the repetitive nor the rpl41a model mRNAs showed significant differences in mRNA binding relative to the initial model

mRNA (Figures 3, S5, and Table S2), demonstrating that mRNA binding by eIF3 species is relatively sequence non-specific in the absence of additional interacting components.

Because the eIF3c C-terminal domain forms a stable heterodimer with the eIF3a N-terminal domain that has been shown to stabilize mRNA binding to the PIC[22,56], we wondered whether the inclusion of eIF3c would affect the high-affinity mRNA binding we observe for eIF3a. Consistent with this possibility, eIF3a and eIF3c form the highest affinity subcomplex we identified in our mass photometry experiments and could be expected to predominantly form a 3ac subcomplex under our titration conditions (Figure S3B and Table S1). In contrast, assessing whether and to what extent the other subcomplexes can directly interact with mRNA is complicated by the dynamic compositional equilibria of these subcomplexes and free subunits. Even given these complications, we find that inclusion of eIF3c within an eIF3ac subcomplex results in a binding curve that matches nearly identically with that of $eIF3_R$, suggesting that the interaction between eIF3a and eIF3c may modulate the mRNA binding activity of eIF3a (Figure S6A).

eIF3a-containing subcomplexes drive the reported mRNA binding activity of eIF3

The dynamic compositional equilibrium of eIF3 complicates the analysis and interpretation of mRNA-binding experiments because it invalidates assumptions inherent to two-component, single-site binding models. These models underlie the approaches that are most frequently used to analyze data from such experiments and have been employed as simplifying assumptions in all previous studies of eIF3[22,36]. In contrast, mRNA binding by eIF3a is strictly bimolecular and therefore should more closely obey the assumptions of a two-component, single-site binding model than mRNA binding by $eIF3_N$ or $eIF3_R$. Furthermore, our fluorescence anisotropy data at concentrations below 50 nM for eIF3a alone, $eIF3_N$, and $eIF3_R$ are similar but deviate at higher concentrations (Figures 3A, S5B, and S5D). At these lower concentrations, $eIF3_N$ and $eIF3_R$ contain a significant amount of free subunits, including eIF3a (Figures 1A and 1B), and thus we hypothesized that eIF3a might be primarily responsible for the observed mRNA-binding activity of eIF3 to mRNA in all cases and that the compositional heterogeneity of $eIF3_N$ and $eIF3_R$ could be modulating this activity. We therefore sought to directly test how the dynamic compositional equilibrium of eIF3 alters its observed mRNA-binding activity.

We first tested this using fluorescence anisotropy binding experiments where we increased the concentration of total mRNA in separate titrations. As the concentration of mRNA is increased, the amount of eIF3a or eIF3 required to saturate binding should increase if the assumptions of two-component, single-site binding are correct. This should shift the binding curve to higher concentrations and, at concentrations near and above the K_d, result in a non-hyperbolic titration curve[61]. Because we have full control over the subunit stoichiometry of $eIF3_R$ and not $eIF3_N$, we performed these experiments comparing eIF3a and $eIF3_R$. As expected, when we increased the concentration of mRNA and performed binding experiments with eIF3a alone, the resultant plots of normalized anisotropy match closely with those modeled by a two-component, single-site binding model (Figure S7A). Strikingly, identical experiments with $eIF3_R$ as the titrant do not show this trend (Figure S7B). Rather, these binding curves saturate at concentrations > 500 nM $eIF3_R$ regardless of the mRNA concentration, followed by a decrease in anisotropy that continues as $eIF3_R$ concentrations increase. Notably, this decrease in anisotropy at higher eIF3 concentrations is also observed when $eIF3_N$ is the titrant (Figure 3A). These decreases in anisotropy led us to consider whether the dynamic compositional equilibrium of eIF3 at higher protein concentrations was leading to the accumulation of species that bind the mRNA with relatively low affinity. In other words, these observations suggested the possibility that the full eIF3 complex or other subcomplexes may exhibit a lower affinity for mRNA. This hypothesis, that the accumulation of specific eIF3 subspecies might regulate the affinity with which eIF3 binds mRNA is consistent with our observation that the inclusion of eIF3c to form the eIF3ac subcomplex alters the mRNA binding of the complex relative to eIF3a or eIF3c in isolation (Figure

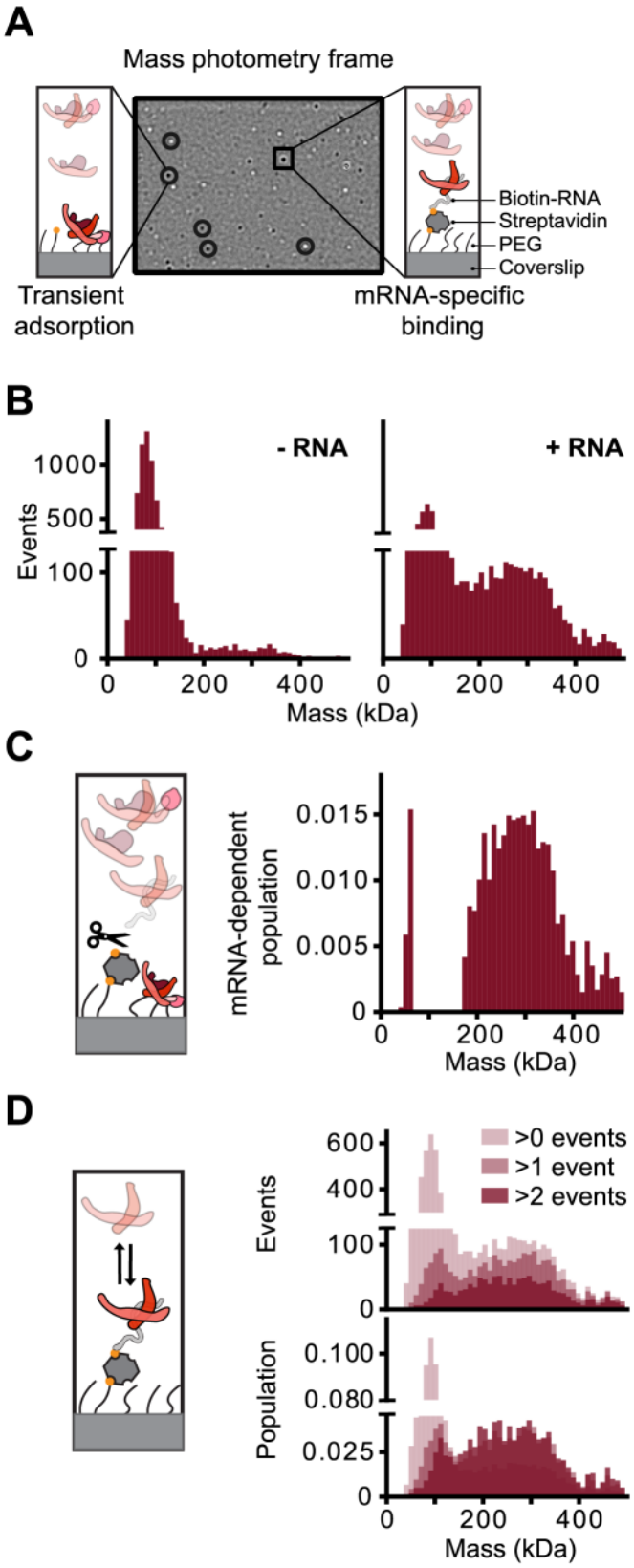

Figure 4. Distinguishing between transient adsorption and mRNA-specific binding events in mass

photometry. (A) *An example frame from mass photometry depicting various events in the field of view. A cartoon illustrating events of transient adsorption to the surface (left) and mRNA-specific binding events (right).* ***(B)*** *Histograms of the mass distribution from mass photometry experiments of 200 nM eIF3$_R$ using derivatized coverslips in the absence (left) and presence (right) of tethered mRNA.* ***(C)*** *The difference mass distribution of 200 nM eIF3$_R$ generated by subtracting the distribution obtained after RNase treatment from that generated before RNase treatment.* ***(D)*** *The mass distribution of 200 nM eIF3$_R$ exhibiting > 0, 1, or 2 events per pixel shown as either raw counts (top) or a normalized population (bottom).*

S6A). Such a hypothesis is exceedingly difficult to experimentally verify with conventional approaches due to various technical challenges: (*i*) the probabilities with which specific subspecies in a dynamic compositional equilibrium of a multi-component complex become available for binding vary non-linearly as a function of concentration, (*ii*) the binding of specific subspecies to the target result in further changes to these probabilities, (*iii*) each subspecies may differentially contribute to the signal response in assays commonly used to measure binding (*e.g.*, components with different masses will contribute differently to the change in anisotropy signal upon binding), and (*iv*) ensemble averaging complicates deconvolution of *i-iii* using ensemble binding assays.

To overcome these difficulties and test this hypothesis directly, we adapted our mass photometry approach to use sample wells in which the borosilicate glass surface is derivatized with a mixture of polyethylene glycol (PEG) and biotinylated (biotin)-PEG (*i.e.*, PEG-derivatized) in a manner similar to the flow cells commonly employed in single-molecule florescence microscopy experiments[44,62-64] (Figure 4A). Derivatization of the surface in this way enables us to sparsely tether a 3'-biotinylated version of the model RNA we previously employed in our PIC-binding and mRNA-binding experiments within each sample well using a biotin-streptavidin-biotin bridge. While mass photometry experiments using conventional, underivatized sample wells report on the masses of biomolecules that irreversibly and non-specifically adsorb across the entire coverslip surface, mass photometry experiments using our PEG-derivatized and tethered-mRNA sample wells report instead on the masses of only those eIF3 species that reversibly and specifically bind to these sparsely tethered, single mRNA molecules (Figure S8A, STAR*methods).

We began these mRNA-binding mass photometry experiments by comparing the adsorption events we observed upon delivering 200 nM eIF3$_R$ to PEG-derivatized wells in either the absence or presence of tethered mRNA. Under both conditions, the distribution of all detected adsorption events yielded a single large peak centered around an apparent mass of 150 kDa (Figure 4B). Because it is present in both the absence and presence of mRNA and does not correspond to any subunit, subcomplex, or the full complex, and is also present in experiments containing buffer alone, we interpret this peak as an artifact inherent to the PEG-derivatized wells (*e.g.*, potential sources of this could be laser-induced heating of the PEG surface, release of physio-adsorbed PEG from the surface, *etc.*). Uniquely in the presence of mRNA, however, we observe a second, broader peak centered at a molecular mass of 250 kDa that we hypothesized represents the binding of eIF3$_R$ components to mRNA. To confirm this hypothesis, we used two independent methods. In the first method, we reasoned that events resulting from specific binding to the mRNA would be sensitive to ribonuclease (RNase) treatment. Thus, we repeated this experiment in the absence and presence of RNase and compared the distribution of all events observed in a well to the distribution of all events observed in the same well, but after adding RNase (Figure 4C). Subtraction of the events detected after RNase addition from those detected before RNase addition leaves only those events that are mRNA-dependent (Figure 4C and S9A). In the second method, we similarly reasoned that only those locations in the mass photometry image containing a tethered mRNA would exhibit multiple adsorption-desorption events, reporting on the reversible binding of eIF3 species to the mRNA, with dissociation events detected as those in which the amount of Rayleigh scattering decreases rather than increases. In contrast, locations

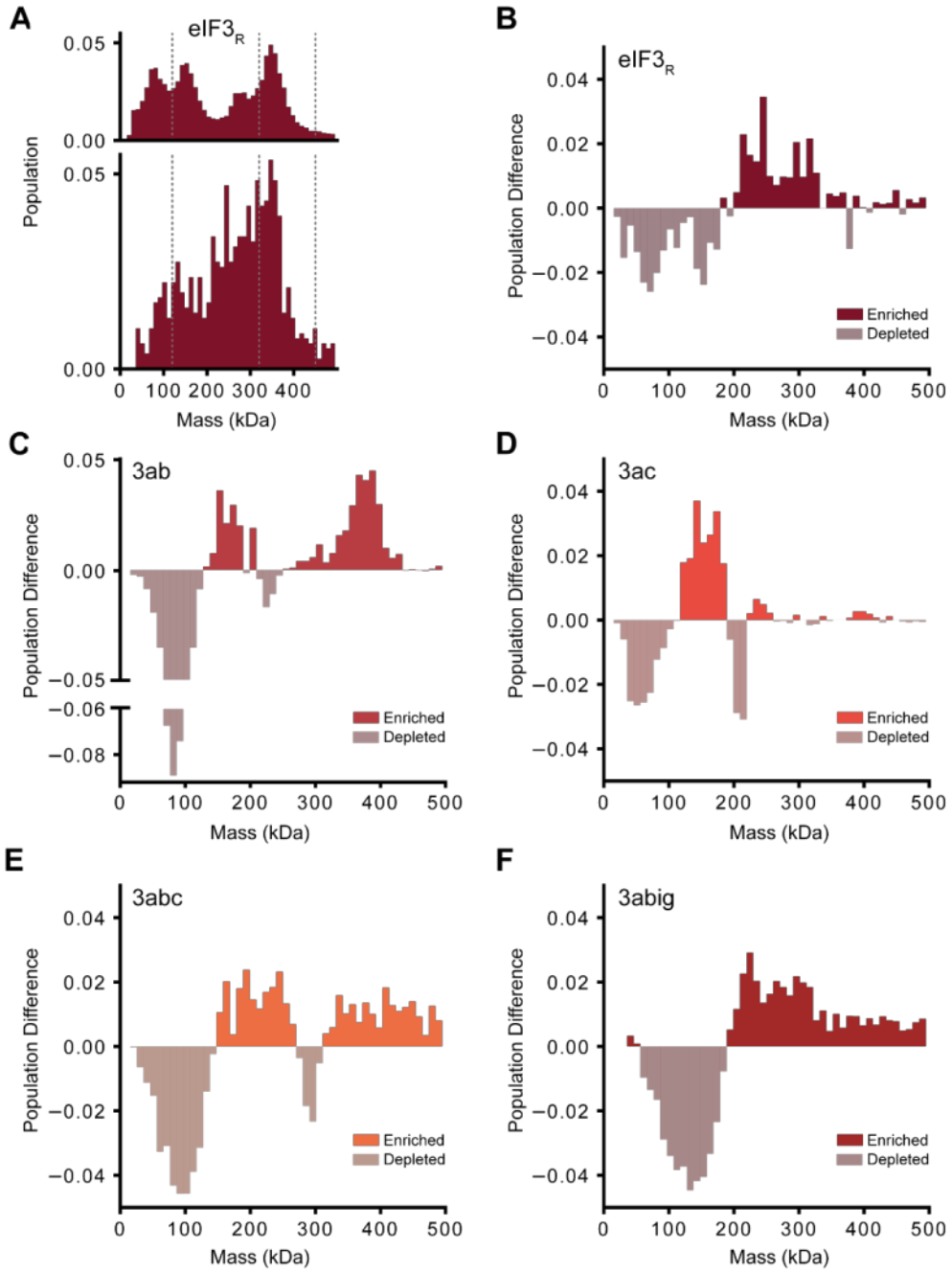

Figure 5. Comparison of the solution mass distribution to the mRNA-binding mass distribution reveals eIF3a-containing subcomplexes differentially bind mRNA. (A) *Solution mass distribution histogram (top) and the mRNA-binding mass distribution (bottom) of 30 nM eIF3R.* ***(B)*** *A population difference plot of the mRNA-binding mass distribution relative to the solution mass distribution for 30 nM eIF3R.* ***(C-F)*** *Population difference plots for eIF3a-containing subcomplexes at 30 nM: 3ab (C), 3ac (D), 3abc (E), and 3abig (F).*

lacking a tethered mRNA would only exhibit a single adsorption or desorption event, as they arise from spurious, potentially PEG-related events detected at the surface. We therefore altered our analysis approach to consider only those locations in the images at which we observed multiple adsorption-desorption events (Figure 4D). Strikingly, both methods for identifying mRNA-

dependent binding events yield similar mass distributions of the $eIF3_R$ species that specifically bind to mRNAs (*i.e.*, the mRNA-binding mass distribution). Unexpectedly, the mRNA-binding mass distribution was very broad and encompassed the masses of eIF3 subcomplexes and the full complex (Figure 4D). Because we have determined the solution mass distribution of $eIF3_R$ in at 30 nM, we repeated the mRNA-binding mass photometry experiment at 30 nM $eIF3_R$ and compared this distribution (built using events detected only at those image locations exhibiting > 2 adsorption-desorption events) to the solution mass distribution in the absence of mRNA (Figure 5A). To identify which eIF3 species bind mRNA and whether these are enriched or depleted in the mRNA-binding mass distribution as compared to the solution mass distribution in the absence of mRNA, we calculated the population difference between these two distributions (Figure 5B). Species that are equally represented in both distributions should yield peaks near zero, whereas enriched or depleted species appear as positive or negative peaks, respectively. This analysis reveals that high-molecular-mass subcomplexes and the full complex exhibit substantial affinity for the mRNA, while low-molecular-mass subcomplexes and subunits do not. The lack of low-molecular-mass subcomplexes and subunits in the mRNA-binding mass distribution, despite their prominence in the solution mass distribution, demonstrates that eIF3a, which we have shown tightly binds mRNA (Figure 3), is rapidly depleted from the low-molecular-mass species and incorporated into higher-molecular-mass species that are capable of mRNA-binding.

A deeper comparison of the mRNA-binding and solution mass distributions demonstrates that relatively high-molecular-mass, eIF3a-containing subcomplexes compete with, and may even outcompete, the full complex for mRNA binding. This can be readily concluded from the observation that the high-molecular-mass subcomplexes are enriched relative to the full complex in the population difference plot (Figure 5B). Consistent with this conclusion, while the concentration limits of mass photometry prevent us from determining the solution mass distribution at elevated concentrations in which the full complex is favored over subcomplexes, analysis of the mRNA-binding mass distribution at 200 nM $eIF3_R$ shows that certain higher-molecular-weight subcomplexes more effectively compete with the full complex for mRNA binding (Figure S8A). This result suggests that, by increasing the total concentration of eIF3 components, the compositional equilibrium of eIF3 is shifted so as to favor the formation of these mRNA-binding, higher-molecular-weight subcomplexes.

Our unique ability to compare the mRNA-binding and solution mass distributions provides an opportunity to identify the binding preferences of all possible subcomplexes. Given our observation that eIF3a appears to be the primary driver of mRNA binding, we sought to narrow the list of possible subcomplexes by testing the ensemble of subcomplexes that form in the absence of eIF3a (*i.e.*, eIF3b+c+i+g) (Figures S3B and S8B). The results of these experiments show that excluding eIF3a largely abolishes the formation of high-molecular-mass subcomplexes as well as mRNA binding. We therefore limited our studies of the remaining subcomplexes to only those containing eIF3a. A comparison of the mRNA-binding and solution mass distributions of all eIF3a-containing subcomplexes shows that each of these subcomplexes binds mRNA to varied extents (Figure 5C-F), although current limitations in the quantitative capabilities of mass photometry prevented us from quantifying these affinity differences. Based on these results, we conclude that eIF3a is necessary and sufficient for eIF3 to bind mRNA. Nonetheless, because eIF3a-containing subcomplexes exhibit differential mRNA binding affinity, and several of these appear to outcompete the full complex for binding (Figure 5B), we further conclude that binding of other eIF3 subunits to eIF3a modulates the mRNA binding affinity of eIF3a within eIF3a-containing subcomplexes.

DISCUSSION

Our work establishes that the full eIF3 complex is in a dynamic compositional equilibrium with its constituent subcomplexes and subunits, and that this dynamic equilibrium governs mRNA binding

by eIF3. We show that the eIF3a subunit is the primary driver of mRNA binding by the yeast core eIF3 complex and that the interactions of eIF3a with eIF3c and other eIF3 subunits modulate its association with mRNA. Most importantly, even at eIF3 concentrations employed in previous biochemical studies[22,44,51-53] and that favor formation of the full eIF3 complex, we observe substantial mRNA binding by eIF3a-containing subcomplexes. These findings indicate that the dynamic exchange of eIF3 subunits has functional consequences for eIF3-mediated mRNA binding under physiological conditions.

We propose a model for eIF3 function that provides a molecular framework for investigating the numerous roles ascribed to eIF3 in translation (Figure 6). In our model, eIF3 is in dynamic exchange between the full complex, distinct subcomplexes, and individual subunits. Free subunits are rapidly sequestered into subcomplexes, largely through their interactions with eIF3a[6,47,65]. Consequently, the most predominantly sampled eIF3 species are the subcomplexes and full complex. Using this framework to characterize how eIF3 interacts with mRNA, we find that eIF3a is both necessary and sufficient for high-affinity mRNA binding, leading to a competition between eIF3a-containing subcomplexes and the full complex for binding sites on mRNA. Interestingly, some eIF3a-containing subcomplexes may bind mRNA less tightly than the full complex does, whereas other eIF3a-containing subcomplexes bind it more tightly. This finding demonstrates that inter-subunit interactions within eIF3 subcomplexes and the full complex can modulate the activities of individual subunits and, in the case of the mRNA binding by eIF3, shows

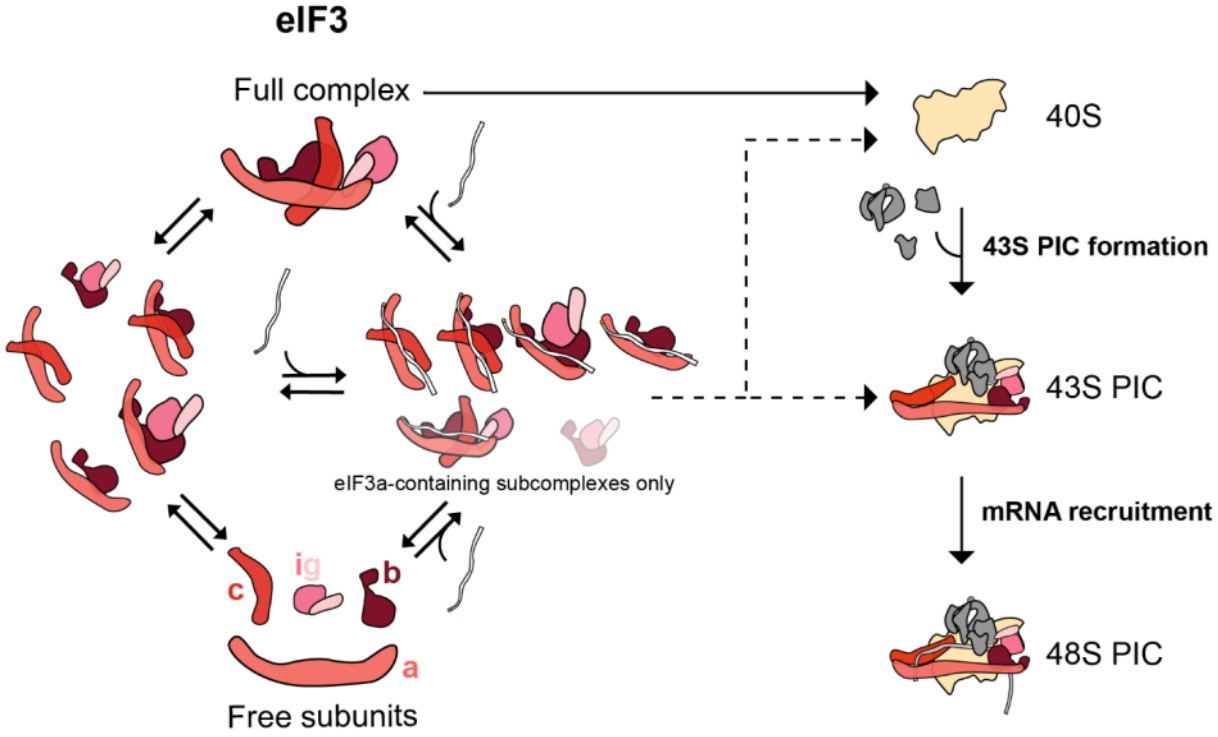

Figure 6. A molecular framework for modulation of eIF3 function by its underlying compositional equilibrium. *In contrast to existing as a stable, compositionally uniform protein complex, eIF3 exists in a dynamic equilibrium between the full complex, various subcomplexes, and free subunits. Additional eIF3-interacting factors likely alter this complex and dynamic compositional equilibrium. The presence eIF3a is required to enable mRNA binding by eIF3 subcomplexes, and eIF3a-containing subcomplexes may bind mRNA with a higher affinity than the full complex. The presence of mRNA thus biases the eIF3 compositional equilibrium to the formation of mRNA-bound eIF3a-containing subcomplexes, which may enable the delivery of mRNAs to free 40S subunits or PICs. Additional modulation of this compositional*

equilibrium may enable the formation of specific eIF3a-containing subcomplexes capable of dictating the translational fates of specific mRNAs.

how certain subcomplexes may outcompete the full complex, even under conditions that otherwise strongly favor formation of the full complex.

Our model predicts two key regulatory routes through which the activities of eIF3 may be controlled. First, the degree to which individual subcomplexes or subunits partition between interacting with additional eIF3 subunits or translational components could be context-dependent, creating a regulatory paradigm in which the presence and concentration of additional translation components can modulate these compositional equilibria and, consequently, the functions of eIF3. As a physiologically important example of this, here we show how the interaction of mRNA with eIF3a-containing subcomplexes modulates these equilibria (Figure 6). In the presence of high concentrations of mRNA, we expect eIF3a-containing subcomplexes to associate with mRNA. This mRNA association would deplete the mRNA-free, higher-order complexes. Consequently, re-equilibration would result in two pools enriched in the following eIF3 species: mRNA-bound, eIF3a-containing complexes, and mRNA- and eIF3a-free complexes (*i.e.*, eIF3big and eIF3ig).

In the second regulatory route predicted by our model, interactions between the translation machinery and individual subunits within the full complex may up- or downregulate the activities of individual subunits. Such interactions could modulate the dynamic eIF3 compositional equilibrium in a manner similar to that described above for mRNA binding in order to control additional eIF3-modulated steps in the initiation pathway, including PIC binding and mRNA recruitment, as well as more expanded activities, for example the recruitment of specific mRNAs, an activity that has been suggested from studies of eIF3 in higher eukaryotes[10,12,13,25]. Perhaps most excitingly, our model raises the possibility that, rather than stimulating translation initiation through the activity of the full complex, perhaps eIF3 accomplishes this through the action of different subcomplexes and subunits that act at different points along the initiation pathway.

Our observations that the mRNA binding activity of non-PIC-bound eIF3 is predominantly driven by eIF3a and that binding of other eIF3 subunits to eIF3a to form eIF3a-containing subcomplexes and the full complex can allosterically modulate this activity raises exciting possibilities for the mechanisms through which an mRNA is delivered to, loaded on, and then scanned by a PIC. One such possibility is that a complex between an mRNA-bound eIF3a-containing subcomplex and mRNA is delivered directly to an otherwise factor-bound PIC, serving a major role in mRNA delivery to the PIC. Although we cannot discount this possibility, a more likely mechanism is one in which mRNA delivery is handled by the eIF4F mRNA-activation complex[4,5] and the mRNA-binding activity of eIF3a within the context of a PIC-bound, eIF3a-containing subcomplex or the full eIF3 complex is allosterically modulated in a manner that facilitates mRNA loading and/or scanning. Such a mechanism is supported by earlier studies attempting to reconstitute eIF3, which proposed allosteric modulation of the structure of eIF3 by the PIC[40]. Given that PIC-bound eIF3a spans both the mRNA-entry and -exit channels[20,22] and serves as the only physical connection between the domains of eIF3 at these two locations on the PIC[6], it is perhaps not surprising that eIF3a would play a central role in interacting with mRNA and in allosteric control of eIF3 activity. Beyond eIF3a, the numerous additional contacts that eIF3 makes with the PIC create additional opportunities for allosteric control of other aspects of translation initiation by eIF3. Such opportunities are likely even further expanded in the case of higher eukaryotes, where an additional seven subunits of eIF3 are present[6,9,35]. Notably, these additional subunits are concentrated at the mRNA-exit channel[49,66,67]. This observation strongly suggests that whatever the expanded functions of these subunits may be, such roles are spatially localized to this region of eIF3 and/or the PIC and likely contribute to a narrowed set of mechanistic or regulatory steps in the initiation pathway of higher eukaryotes.

LIMITATIONS OF STUDY

A caveat to mass photometry is that the laser used for detection heats the sample, limiting the amount of time each field of view can be imaged, which has unknown effects on our derivatized coverslips, and required us to take a higher number of shorter movies as compared to underivatized coverslips (Figure S9C and STAR*Methods).

Several prior studies have suggested that eIF3 interacts with specific mRNAs dependent on sequence[12-18]**.** Seemingly in contrast, our anisotropy experiments testing the ability of eIF3 to bind a limited set of three mRNAs with distinct sequence content did not show a substantial difference in K_d^{app}. However, as we note above, it is possible that these observations could change in the context of PIC-bound eIF3. Moreover, these experiments did not test the binding of eIF3 to more complex mRNAs (*e.g.*, natural mRNAs with long or structured 5'-untranslated-region sequences or with post-transcriptional modifications, *etc.*). As a consequence, it is always possible that the binding affinity of eIF3a, eIF3a-containing subcomplexes, or other eIF3 subunits or subcomplexes, is altered in the presence of a unique set of mRNAs not tested in our study. Furthermore, additional mRNA-binding proteins present in the cell, but not in our *in vitro* experiments, may interact with eIF3 and modulate its apparent mRNA-binding activities.

ACKNOWLEDGEMENTS

This work was supported by funds to R.L.G. and C.E.A. from the NIH (R01 CA277727, R35 GM153724, and R01 GM084288 to R.L.G and R15 GM140372 to C.E.A.). R.C.G. and N.A.I. were supported by NSF GRFP fellowships (DGE-1644869 and DGE-2036197, respectively). E.W.H. was funded through an F32 fellowship from the NIH (F32 GM139360). The authors would like to thank Eric Greene for his thoughtful and critical suggestions on the manuscript, the Columbia Precision Biomolecular Characterization Facility (PBCF) for access to instrumentation, and the PBCF Manager, Dr. Jerry Chang, for assistance with PBCF instrumentation.

AUTHOR CONTRIBUTIONS

Conceptualization, N.A.I., R.C.G., C.D.K.-T., R.L.G., and C.E.A.; Methodology, N.A.I., R.C.G., C.D.K.-T., R.L.G., and C.E.A.; Investigation, N.A.I., R.C.G., and M.A.R.; Resources, N.A.I., R.C.G., V.M.C., K.Y., and E.W.H.; Validation, N.A.I., R.C.G., M.A.R., and P.K.V.; Writing – Original Draft, N.A.I., R.C.G., R.L.G., and C.E.A.; Writing – Review & Editing, N.A.I., R.C.G., R.L.G., and C.E.A.; Supervision, R.L.G. and C.E.A.; Funding acquisition, R.L.G. and C.E.A.

COMPETING INTERESTS

The authors declare no competing interests.

RESOURCE AVAILABILITY

Lead Contact

Further information and requests for resources and reagents should be directed to and will be fulfilled by either of the corresponding authors, Ruben L. Gonzalez, Jr. (rlg2118@columbia.edu), and/or Colin Echeverría Aitken (caitken@vassar.edu).

Materials Availability

All unique and stable reagents generated in this study are available from either of the corresponding authors with a completed Materials Transfer Agreement.

Data and Code Availability

The original source data are available upon request to the corresponding authors.

EXPERIMENTAL AND SUBJECT DETAILS

Yeast Strains

40S subunits were purified from a wild-type, W303 *S. cerevisiae* strain, LSY679 (*MATα leu2-3,112 trp1-1 ura3-1 can1-100 ade2-1 his3-11,15 RAD5)*, a kind gift from L. Symington (Columbia University). eIF3 was natively purified from *S. cerevisiae* strain, LPY87 (pLPY-PRT1His-TIF34HA-TIF35Flag/pLPY-TIF32-NIP1 in *MATa/α ura3-52/ura3-52 trp1/ trp1 leu2-Δ1/leu2-Δ1 his3-Δ200/his3-Δ200 pep::HIS4/pep::HIS4 prb1-Δ1.6/prb1-Δ1.6 can1/can1 GAL*$^{+}$).[32] eIF2 was natively purified from *S. cerevisiae* strain GP3511 (pAV1089[*SUI2 SUI3* His-tagged *GCD11 URA3*] in *MATα leu2-3 leu2-112 ura3-52 ino1 gcn2Δ pep4::LEU2 sui2Δ HIS4-lac*).[68]

Bacterial Strains

All recombinant protein overexpression was performed in *Escherichia coli* BL21-CodonPlus (DE3)-RIPL cells (Agilent, Catalog Number 230280, F– ompT hsdS(rB – mB –) dcm+ Tetr gal l(DE3) endA Hte [argU proL Camr] [argU ileY leuW Step/Specr]). All cloning was performed using NEB DH5*α* (New England Biolabs, Catalog Number C2987H, *fhuA2Δ(argF-lacZ)U169 phoA glnV44 Φ80Δ(lacZ)M15 gyrA96 recA1 relA1 endA1 thi-1 hsdR17*).

METHOD DETAILS

Cloning, Expression, and Purification of Recombinant eIF3 Subunits

The expression plasmids used for eIF3a and eIF3b are identical to those previously reported[40]. The expression plasmid for eIF3c contains an N-terminal, six-histidine (6× His) tag, followed by a *Fasciola hepatica* 8 kDa (Fh8) solubility enhancer tag[69], a tobacco etch virus (TEV) protease recognition site. This results in a full-length, untagged eIF3c with no residual scar from the TEV cleavage site. The expression plasmid for eIF3i-eIF3g is identical to that previously reported[40], with the exception that the PreScission protease cleavage site between eIF3i and eIF3g was changed to a TEV protease cleavage site.

The expression protocol for each recombinant eIF3 subunit was as follows. Each subunit was overexpressed from a pET vector (Novagen) in *E. coli* BL21-CodonPlus (DE3)-RIPL cells (Agilent, Catalog Number 230280). Cells were grown at 37 °C to an optical density at 600 nm (OD_{600}) of 0.4-0.6. The temperature was then lowered to 17.5 °C. After 45-60 min, expression was induced by addition of 0.5 mM isopropyl ß-D-1-thiogalactopyranoside (IPTG) and the cells were grown overnight (16-20 hours). The next morning, these cell cultures were cooled by placing them in a plastic autoclave bin filled with ice and the cells were pelleted by repeated centrifugation at 8,000 relative centrifugal force (rcf) for 5 minutes. Pelleted cells were resuspended in 40-50 mL of eIF3 Lysis Buffer (20 mM 4-(2-hydroxyethyl)-1-piperazine ethanesulfonic acid (HEPES) at a pH of 7.4, 400 mM potassium chloride (KCl), 10% glycerol, and 2 mM β-mercaptoethanol (βME)). The cell slurry was then flash frozen as droplets by slowly dropping the slurry into a bowl filled with liquid nitrogen. The resulting frozen droplets can be stored at –80 °C for at least 2

months. These droplets were then lysed using a freezer mill (SPEX, Catalog Number 6875D115) using 7 cycles of 2 minutes on-time at a rate of 10 cycles per second, followed by 1 minute of off-time. The resulting lysate powder was then stored at –80 °C.

To begin each purification, the lysate powder was resuspended in 100-200 mL of room temperature eIF3 Lysis Buffer supplemented with 2 ethylenediamine tetraacetic acid (EDTA)-free protease inhibitor tablets (Roche, Catalog Number 04693132001), 20 mM imidazole, 10 mM magnesium chloride ($MgCl_2$) and 50 µg of nuclease A from *Serratia marcescens* by slowly adding the powder to actively stirring eIF3 Lysis Buffer in a 0.5 L glass beaker. The lysate was then clarified at 31,500 rcf for 30 minutes and the supernatant was filtered through a 0.45-micron bottle-top filter before loading onto a HiTrap 5 mL chelating column (Cytiva, Catalog Number 17040901) that had been charged with nickel sulfate ($NiSO_4$) according to the manufacturer's instructions and pre-equilibrated with K-200 Buffer (20 mM HEPES at a pH of 7.4, 200 mM KCl, and 10 % glycerol). The subunit was then eluted using an 8× column-volume (c.v.) gradient of K-200 Buffer supplemented with 400 mM imidazole. Up to this point, the preparation for each subunit was identical. The next steps, which were unique to each subunit, are detailed in the following paragraphs.

For eIF3a and eIF3b, the entire volume eluted from the HiTrap 5 mL chelating column was pooled, diluted 2-fold in K-200 Buffer, and subsequently loaded onto a HiTrap Q 5 mL column (Cytiva, Catalog Number 17115401) that was in-line connected to a second HiTrap Q 5 mL column and that were pre-equilibrated with K-200 Buffer. The protein was eluted using a 15× c.v. gradient of K-1000 Buffer (20 mM HEPES at a pH of 7.4, 1,000 mM KCl, and 10% glycerol). For both eIF3a and eIF3b, there is largely a single, homogenous peak upon elution. The purities of the fractions were validated using sodium dodecyl sulfate-polyacrylamide electrophoresis (SDS-PAGE) followed by staining with Coomassie brilliant blue. The fractions with a single band corresponding to the molecular mass of the desired recombinant protein were pooled and the concentration of the protein was determined using a Bradford assay with bovine serum albumin as a standard. The protein was then aliquoted into 10 µL single-use aliquots and flash frozen in liquid nitrogen.

For eIF3c, the peak from the HiTrap 5 mL chelating column elution corresponding to eIF3a was pooled and treated with 1:100 (w/w) TEV protease and 2 mM βME. For efficient proteolysis of the Fh8 enhanced solubility tag, this mixture was incubated at room temperature for 2-3 hours followed by a further incubation at 4 °C overnight. The next day, this mixture was diluted 10-fold in K-200 Buffer in order to lower the concentration of imidazole. After dilution, to remove the TEV protease and any uncleaved Fh8-eIF3c, the mixture was passed through a HiTrap 5 mL chelating column freshly recharged with $NiSO_4$ and pre-equilibrated with K-200 Buffer. The flow-through was then pooled, loaded onto, and eluted from 2 HiTrap Q 5 mL columns in-line connected in a manner identical to that described for eIF3a and eIF3b above. As above, the purity of the fractions was validated using SDS-PAGE and the appropriate fractions were pooled prior to aliquoting and flash freezing.

For eIF3i-eIF3g, the peak from the HiTrap 5 mL chelating column elution was pooled and then diluted 2-fold using K-200 Buffer. The diluted protein fusion was then loaded onto, and subsequently eluted from, 2 HiTrap Q 5 mL columns in-line connected as described above. This peak was then pooled and, in order to cleave the eIF3i-eIF3g protein fusion, TEV protease and βME were added to final concentrations of 1:100 (w/w) TEV protease and 2 mM βME. For efficient proteolysis, this mixture was incubated at room temperature for 2-3 hours followed by further incubation at 4 °C overnight. The next day, TEV protease was removed by loading this mixture onto a Superdex 200 Increase 10/300 GL column (Cytiva, Catalog Number 28990944) that had been equilibrated in K-200 Buffer and was eluted using additional K-200 Buffer as a running buffer. As described above for the other subunits, the purity of the fractions was checked using SDS-PAGE, the appropriate fractions were pooled, the concentration was determined, and single-

use aliquots were flash frozen. Importantly, any fractions containing detectable uncleaved eIF3i-eIF3g protein fusion were removed prior to pooling.

Purification of eIF3$_N$

Native *S. cerevisiae* eIF3 was expressed using strain LPY87 as previously described[32,37,38]. Briefly, LPY87 was grown on selective media plates lacking uracil and leucine for 2-3 nights at 30 °C. A 50-100 mL starter culture was grown in liquid selective media overnight at 30 °C. After 16-20 hours, 5 mL of this starter culture was added to 1.5 L of yeast extract peptone dextrose (YPD) media and grown overnight again at 30 °C. The cells from these overnight cultures were then pelleted, resuspended, flash frozen, and lysed in eIF3 Lysis Buffer as described above.

To begin the eIF3$_N$ purification, the lysate was loaded onto and eluted from a HiTrap 5 mL chelating column charged with a $NiSO_4$ solution in a manner identical to that described for the recombinant subunits above.

The entire elution from the HiTrap 5 mL chelating column was pooled, diluted 2-fold in K-200 Buffer, and then loaded onto 2 HiTrapQ 5 mL columns in-line connected as described above. In an attempt to separate eIF3 complexes contaminated with eIF5 from those without eIF5[20], a shallow elution gradient was used; specifically, a 20× c.v. gradient between 0-50 % of K-200 Buffer and K-1000 Buffer. This elution resulted in two major peaks: one centered at a conductivity of 25 mS/cm and another, much broader peak, at a conductivity of > 27 mS/cm. The fractions corresponding to both peaks were analyzed using SDS-PAGE. Surprisingly, each fraction seemed to contain a population of full eIF3 complexes with varying levels of contamination. The fractions corresponding to the peak at 25 mS/cm were pooled and, separately, the fractions corresponding to the peak > 27 mS/cm were pooled. Each of these two mixtures were then separately loaded onto a Superose 6 Increase 10/300 column (Cytiva, Catalog Number 29091596) equilibrated in K-200 Buffer and eluted using additional K-200 Buffer as a running buffer. Each mixture resulted in two major peaks, one corresponding to a larger molecular mass complex and the other corresponding to a smaller molecular mass complex. However, the mixture containing the fractions corresponding to a conductivity of > 27 mS/cm produced a significantly larger population of the larger molecular mass complex. Therefore, only the fractions from the peak corresponding to the larger molecular mass complex obtained from the mixture containing the fractions corresponding to a conductivity of > 27 mS/cm were pooled and analyzed by SDS-PAGE to confirm the presence of the five core eIF3 subunits. As above, the concentration was determined using a standard Bradford assay and the sample was aliquoted into 10 µL single-use aliquots and flash frozen in liquid nitrogen.

Purification of eIFs 1, 1A, 2, 4GE, 4A, and 4B

eIF1, eIF1A, and eIF4A were expressed with N-terminal 6× His tags followed by a TEV protease cleavage site. eIF4B was expressed with a C-terminal TEV protease cleavage site followed by a 6× His tag. These factors were purified from *E. coli* BL21(DE3) RIPL cells (Agilent, Catalog Number 230280) following established procedures[36-38]. Native, 6× His-tagged eIF2 was expressed and purified from *S. cerevisiae* strain GP3511 as previously described[37]. eIF4G containing a C-terminal TEV protease cleavage site followed by an Fh8 tag and 6× His tag was co-expressed with full-length eIF4E. This results in an eIF4GE complex, which was purified from *E. coli* BL21(DE3) RIPL cells (Agilent, Catalog Number 230280) as previously described[44].

Purification of 40S Subunits

Native *S. cerevisiae* 40S subunits were purified from a wild-type, W303 *S. cerevisiae* strain, LSY679, largely following established protocols[37] with the deviations outlined here. First, cells were grown at 30 °C to an OD_{600} of 0.8-1.2, then pelleted, resuspended in Ribosome Lysis Buffer (20 mM HEPES at a pH of 7.4, 100 mM potassium acetate (KOAc), 7.5 mM $Mg(OAc)_2$, and 5 mM

βME), and flash frozen as droplets in liquid nitrogen. The frozen droplets were then lysed in a freezer mill as described above.

To begin the purification, the lysate powder was resuspended in 50-200 mL of room temperature Ribosome Lysis Buffer supplemented with 2 EDTA-free protease inhibitor tablets (Roche, Catalog Number 04693132001), Turbo DNAse (Invitrogen, Catalog Number AM2239), and 0.5-1 mg/mL heparin. The resuspended lysate was then clarified at 31,500 rcf for 30 minutes. A High-Salt Sucrose Cushion Buffer (20 mM HEPES at a pH of 7.4, 100 mM KOAc, 500 mM KCl, 2.5 mM $Mg(OAc)_2$, 34 % w/v sucrose, and 5 mM βME) was then layered underneath the supernatant of the clarified lysate. 80S ribosomes were then pelleted through the High-Salt Sucrose Cushion Buffer by ultracentrifugation at 60,000 rpm in a Ti 70 rotor (Beckman Coulter, Catalog Number 337922) for 2 hours at 4 °C. After the spin, the ribosome pellets were rinsed with 1 mL of Subunit Separation Buffer (50 mM HEPES at a pH of 7.4, 550 mM KCl, 2 mM $MgCl_2$, and 5 mM βME) and the centrifuge tubes were left inverted to dry for 10 minutes at room temperature. The pellets were then resuspended in ~400 uL of Subunit Separation Buffer.

The resuspended pellets across all tubes were pooled. To dissociate the the 40S subunits from the ribosomal large, or 60S, subunits, puromycin dihydrochloride (Goldbio, Catalog Number P-600-100) was added to a final concentration of 2 mM and the centrifuge tubes were inverted to mix, placed on ice for 10 minutes, and subsequently moved to a 37 °C water bath for 15 minutes. The mixture of dissociated subunits was then layered on top of a 10-35 % sucrose density gradient prepared using Subunit Separation Buffer supplemented with either 10 % or 35 % sucrose. The subunits were then separated by ultracentrifugation in an SW32 rotor (Beckman Coulter, Catalog Number 369694) at 22,000 rpm for 17 hours at 4 °C.

The next day, the sucrose density gradients were fractionated on a BioComp Instruments Piston Gradient Fractionator™. The fractions from the peaks corresponding to the 40S and 60S subunits were pooled separately and pelleted through a High-Salt Sucrose Cushion Buffer as above. The separated 40S and 60S subunit pellets were resuspended in Subunit Separation Buffer and each of the resulting 40S and 60S subunit samples were run through another 10-35% sucrose density gradient prepared as described above in order to separate any contaminating 40S or 60S subunits from the 60S and 40S subunit samples, respectively. The next day, the 40S and 60S subunit samples were fractionated and pooled as done on the previous day. Each of the subunit samples were then pelleted through a Ribosome Storage Cushion Buffer (20 mM HEPES at a pH of 7.4, 100 mM KOAc, 2.5 mM $Mg(OAc)_2$, 30 % w/v sucrose, and 2 mM dithiothreitol (DTT)). These pellets were resuspended in Ribosome Storage Buffer (20 mM HEPES at a pH of 7.4, 100 mM KOAc, 2.5 mM $Mg(OAc)_2$, 8.5 % w/v sucrose, and 2 mM DTT). The concentration of each subunit sample was determined using absorbance at 260 nm and extinction coefficients at 260 nm (ε_{260nm}s) of 2×10^7 $M^{-1}cm^{-1}$ and 4×10^7 $M^{-1}cm^{-1}$ for the 40S and 60S subunits, respectively[37] before aliquoting into 5 µL single-use aliquots that were flash frozen in liquid nitrogen and stored at –80 °C.

Transcription, Purification, and Aminoacylation of Initiator tRNA

S. cerevisiae initiator tRNA ($tRNA_i^{Met}$) was generated by *in vitro* transcription using T7 RNA polymerase (RNAP). To generate the DNA template, we used the polymerase chain reaction (PCR) to amplify the portion of a pUC19 vector that contained a T7 promoter followed by a hammerhead ribozyme construct and the $tRNA_i^{Met}$ sequence[70]. Because it starts with a 5' guanosine nucleotide, the hammerhead ribozyme construct enabled efficient transcription by T7 RNAP while subsequently allowing self-cleavage of the transcript by incubation at 65 °C for 1 hr after transcription so as to generate the native $tRNA_i^{Met}$ containing an adenosine nucleotide at the 5' end. After cleavage, the hammerhead ribozyme and $tRNA_i^{Met}$ fragments of the transcript were separated using denaturing (D)-PAGE on a 7 % polyacrylamide (19:1 acrylamide:bis-acrylamide) gel prepared in TBE Buffer (90 mM tris-borate and 2 mM EDTA) supplemented with 7 M urea. The $tRNA_i^{Met}$ was then extracted from the gel *via* 'crush and soak'. Briefly, the $tRNA_i^{Met}$ within the

gel was visualized by ultraviolet (UV) shadowing, the corresponding region of the gel containing the $tRNA_i^{Met}$ was excised, and then the excised gel piece was agitated at 4 ºC overnight in a solution of 300 mM sodium acetate at a pH of 5.2, supplemented with 1 mM EDTA. The extracted $tRNA_i^{Met}$ was then concentrated by ethanol precipitation.

The purified $tRNA_i^{Met}$ pellet was dissolved in 10 mM sodium acetate at a pH of 5.2. To fold the $tRNA_i^{Met}$, it was placed into boiling water that was allowed to slow cool to room temperature. Once the sample was near-room-temperature, 5 mM $Mg(OAc)_2$ was added to stabilize the folded $tRNA_i^{Met}$. The folded $tRNA_i^{Met}$ was then used to prepare an Aminoacylation Reaction Mixture (100 mM HEPES at a pH of 7.4, 10 mM $MgCl_2$, 10 mM KCl, 0.1 mM methionine, 10 mM ATP•Mg, 1 mM DTT, 1 μM *E. coli* methionyl-tRNA synthetase, and 12 μM folded $tRNA_i^{Met}$) based on previously established methods for *in vitro* aminoacylation of tRNAs[70]. This mixture was incubated at 37 °C for 30 minutes, followed by phenol-chloroform extraction and ethanol precipitation. The resulting pellet contains significant contaminating ATP, and was therefore resuspended in 10 mM sodium acetate at a pH of 5.2 and run through 3 sequential PD SpinTrap G-25 columns (Cytiva, Catalog Number 28918004) equilibrated in 10 mM sodium acetate at a pH of 5.2, following the manufacturer's protocol. The concentration of the Met-$tRNA_i^{Met}$ was then determined *via* its absorbance at 260 nm and an ε_{260nm} of 708,900 $M^{-1}cm^{-1}$, aliquoted into 5 μL single-use aliquots, flash frozen in liquid nitrogen, and stored at -80°C.

Standard Reaction Buffer

All measurements were performed in a Standard Reaction Buffer (20 mM HEPES at a pH of 7.4, 100 mM KOAc, and 3 mM $Mg(OAc)_2$) that has been previously shown to be optimal for studies of *S. cerevisiae in vitro* translation initiation[22,36-38].

PIC Binding Assays

The abilities of $eIF3_R$ and $eIF3_N$ to bind to PICs were assessed using a native gel electrophoresis-based assay to monitor the mobility of a fluorescein-labeled 'polyCAA' mRNA with the following sequence: GGCAACAACAACAACAACAACAAAUGGAACAACAACAACAAC AAAGUCGA-fluorescein. A 2× PIC Master Mix was prepared by combining 2 μM eIF1, 2 μM eIF1A, 600 nM eIF2, 750 nM Met-$tRNA_i^{Met}$, 100 nM 40S subunit, and 1 μM polyCAA-fluorescein mRNA. This 2× PIC Master Mix was then combined with stock solutions of $eIF3_R$ or $eIF3_N$ and Standard Reaction Buffer to make a series of solutions in which the final conditions were 1 μM eIF1, 1 μM eIF1A, 300 nM eIF2, 375 nM Met-$tRNA_i^{Met}$, 50 nM 40S subunit, 0.5 μM polyCAA-fluorescein RNA, and 10-800 nM $eIF3_R$ or $eIF3_N$, depending on the concentration of $eIF3_R$ or $eIF3_N$ to be tested. Reactions were incubated at 26 °C for 1 hr, after which time 8 μL of the reaction was combined with 1 μL of Native Loading Dye (0.05% bromophenol blue and 50% sucrose in Standard Reaction Buffer) and then loaded onto a 4%, polyacrylamide (37.5:1 acrylamide:bis-acrylamide) gel prepared in THEM Buffer (34 mM Tris Base, 57 mM HEPES, 0.1 mM EDTA, and 2.5 mM $MgCl_2$). This gel was then run for 1 hr at 200 Volts, and maintained at 16 °C with a circulating water cooler[22,37]. Subsequently, the gel was imaged for fluorescein fluorescence on an Amersham Typhoon 5 Biomolecular Imager (Cytiva, Catalog Number 29187191). Because a large excess of the polyCAA-fluorescein mRNA was used to saturate the PIC, the free mRNA signal saturated the corresponding pixels on the imager detector. This saturated signal was therefore ignored, and the fraction of eIF3-bound PICs was calculated using the total PIC concentration (see 'Quantification of eIF3 PIC Binding and mRNA Recruitment Assays' below).

mRNA Recruitment Assays

The kinetics with which a capped rpl41a mRNA was recruited to PICs was determined using a previously described native gel electrophoresis-based assay to monitor the mobility of a [^{32}P]-cap-labeled rpl41a mRNA[22,36,52,53]. A 2× PIC Master Mix was formed by combining 2 μM eIF1, 2 μM eIF1A, 600 nM eIF2, 750 nM Met-$tRNA_i^{Met}$, 4 μM eIF4A, 800 nM eIF4B, 100 nM 40S subunit,

and 4 mM ATP•Mg^{2+}. This 2× PIC Master Mix was then used to generate a 1× reaction by adding stock solutions of $eIF3_R$ or $eIF3_N$ to the final specified concentrations. mRNA recruitment reactions were initiated by adding [^{32}P]-cap-labeled rpl41a mRNA to a final concentration of 15 nM. mRNA recruitment reactions were incubated continuously at 26 °C. At each specified time point, 4 µL of the reaction was removed and combined with 1 µL of Native Loading Dye and loaded onto an actively running 4 % polyacrylamide (37.5:1 acrylamide:bis-acrylamide) gel prepared in THEM Buffer. This gel was then run for 70 min at 200 Volts, and maintained at 16 °C with a circulating water cooler[22,37]. Subsequently, the gel was exposed to a phosphor screen overnight and then imaged on an Amersham Typhoon 5 Biomolecular Imager (Cytiva, Catalog Number 29187191).

mRNA Binding Assays

mRNA binding was assessed using a fluorescence anisotropy-based assay. These assays were performed using chemically synthesized, 3'-fluorescein-labeled model mRNAs (Integrated DNA Technologies), with the following sequences:

- 'polyCAA'=GGCAACAACAACAACAACAACAAAUGGAACAACAACAACAACAAAGUCGA-Fluorescein
- 'polyUC'=GGAAUCUCUCUCUCUCUCUAUGCUCUCUCUCUCUCUCUCUCUC-Fluorescein
- 'Natural'=GGAGACCACAUCGAUUCAAUCGAAAUGAGAGCCAAGUGGAGAAAGAAGAGA- Fluorescein

For each set of affinity experiments, 1 mL of a 5 nM mRNA solution was prepared by supplementing Standard Reaction Buffer with mRNA. In parallel, the highest concentration protein sample (800 nM for $eIF3_R$ or $eIF3_N$ or 2 µM for eIF3 subunits) was also supplemented to 5 nM mRNA. This highest concentration protein sample was then 2-fold serially diluted using the 5 nM mRNA solution to generate all other, lower protein concentration points to the lowest concentration protein samples tested (3.1 nM for $eIF3_R$ or $eIF3_N$ or 7.8 nM for eIF3 subunits). The resulting concentration series was incubated in a black-bottomed, 96-well plate (Corning, Catalog Number 3916) that was placed in the dark and allowed to equilibrate at room temperature for 20 min. The fluorescence polarization of the concentration series in the plate was then measured on a BioTek Synergy Neo2 plate reader (Agilent) using a 485 nm excitation source and an Agilent Green FP filter cube (Agilent, Catalog Number 8040561).

For each set of stoichiometry experiments in the titration regime, the protocol is identical to that described above, with one exception. Briefly, the total concentration of polyCAA mRNA in the experiment was raised to 400 nM. This was achieved by mixing 50 nM of the fluorescein-labeled polyCAA mRNA with 350 nM of its unlabeled counterpart.

Mass Photometry Assays

Conventional mass photometry experiments were performed using a commercially purchased mass photometer (Refeyn, Inc., TwoMP). Borosilicate glass coverslips (Research Products International Corp, Catalog Number 246008) were cleaned by sonication in 100 % ethanol for 15 min, sonicated in 1 M KOH for 15 minutes, and then thoroughly washed with nanopure water and blow-dried with pre-purified argon gas. To generate sample wells, silicone gaskets (Grace Bio-Labs, Catalog Number GBL103250) were placed on the cleaned coverslips. Proteins were diluted to 30 nM in Standard Reaction Buffer prior to measurements, unless otherwise noted. Measurements were acquired as 60-sec movies in the 'regular', 10.9 µm × 4.3 µm field-of-view recorded using the AcquireMP software (Refeyn, Inc.), and the resulting movies were analyzed using the DiscoverMP software (Refeyn, Inc.). Protein masses were determined using a calibration curve that was established using three protein standards taken from a High Molecular Weight Calibration Kit (Cytiva, Catalog Number 28-4038-42): Conalbumin (75 kDa), aldolase (158 kDa), and thryoglobin (669 kDa).

Tethered mRNA mass photometry experiments were performed using derivatized coverslips. To derivatize a coverslip, the borosilicate glass surface was passivated with a monolayer mixture of methoxy-terminated PEG (mPEG, Laysan Bio, Catalog Number MPEGSIL50001G) and biotin-terminated PEG (biotin-PEG, Laysan Bio, Catalog Number Biotin-PEG-SIL-5K-1g) as previously described[44]. To make sample wells, small cups cut from p200 pipette tips were epoxied (Devcon Home, Catalog Number 20945) onto the surface of the coverslip. This was required because the surface of the derivatized coverslip is hydrophilic and therefore the sample leaks under the silicone gaskets used above. Prior to the addition of sample, wells were rinsed with 70 µL of Standard Reaction Buffer followed by 70 µL of Standard Reaction Buffer supplemented to 0.1 % Tween-20 detergent and then subsequently washed 3 times with 70 µL Standard Reaction Buffer. Streptavidin was bound to the biotin-terminated PEGs by addition of 20 µL of 10 nM streptavidin (Invitrogen, Catalog Number S888) and free streptavidin was removed by rinsing the well 4 times with 70 µL Standard Reaction Buffer. A 3'-biotinylated version of the polyCAA mRNA described above (Integrated DNA Technologies) was tethered to the biotin-PEG-bound streptavidin by incubating 10 nM mRNA in the well for 1 min at room temperature and subsequently removing free mRNA by rinsing 5 times with 70 µL Standard Reaction Buffer. To begin each measurement, 20 µL of 2× protein was then mixed with 20 µL of Standard Reaction Buffer in the well and imaged. Measurements were acquired as 10 15-sec movies in the 'regular' field-of-view and masses were determined as described above. After each measurement, 10 ng of nuclease A from *Serratia marcescens* was added to the well and allowed to incubate for 2 min. Following RNase treatment, 10 more 15-sec movies were acquired.

QUANTIFICATION AND STATISTICAL ANALYSIS

Mass Photometry Data Processing

For all mass photometry experiments, the events detected using the DiscoverMP software were exported as 'comma-separated-value' (csv) files. These unprocessed output data are available in the source data included with this manuscript (see Data and Code Availability). Because mass photometry detects both adsorption and desorption events, both adsorption events, denoted as positive masses, and desorption events, denoted as negative masses, are present in the exported events file. Normalized mass distribution histograms were calculated using only those adsorption events with masses between 0 and 500 kDa such that the sum of all the bars in each histogram sum to 1. To identify pixels where multiple events occur, the super-resolution *x*- and *y* coordinates for each event were rounded to the nearest integer and the number of events at each pixel were determined.

To calculate the RNase-dependent mass distribution for each eIF3 species, the normalized mass distribution measured after addition of RNase was subtracted from the normalized mass distribution before addition of RNase. To calculate the population difference between mRNA-binding mass distribution and the solution mass distribution, the mRNA-binding distribution was filtered for events occurring in pixels which exhibited > 2 events and then normalized. The normalized solution mass distribution was then subtracted from this resulting normalized mRNA-binding mass distribution.

Quantification of Solution Mass Distributions Using Thresholds

The initial threshold cutoffs defining the molecular mass ranges corresponding to 'subunits', 'subcomplexes', and the 'full complex' were 0-120, 120-320, and 320-450 kDa and were selected based on the sequence-determined molecular masses of eIF3 subunits and the full complex (Table S1). The population of each species was then calculated by taking the fraction of total adsorption events within the molecular mass range corresponding to that species and dividing it by the total number of adsorption events with positive molecular masses. This process was performed separately for three replicates of each solution mass distribution, and, for each

distribution, the population of each species was reported as the average and standard deviation across the three replicates.

To test how sensitive this threshold-based analysis was to the selection of the particular threshold values, the analysis described above was repeated at two additional sets of molecular mass ranges. In the first set, the molecular mass ranges corresponding to 'subunits', 'subcomplexes', and the 'full complex' were set to 0-100, 100-300, and 300-430 kDa. In the second set, the molecular mass ranges corresponding to 'subunits', 'subcomplexes, and 'full complex' were set to 0-140, 140-340, and 340-470 kDa (Figures S2C and S2D).

Identification of Peak Centers in Solution Mass Distributions Using Mixtures of Gaussians

Gaussian fitting of solution mass distributions was performed on the 30 nM solution mass distributions to identify the mean molecular mass of each peak observed in the distributions. For distributions with single peaks (*i.e.*, the eIF3 samples containing individual subunits), the mean of the Gaussian distribution was calculated by fitting to a Gaussian function with the 'fitdisr()' function from the 'MASS' library in R, version 4.2.3.[71] No initial guesses were provided. For distributions with multiple peaks, the mean of each Gaussian distribution was calculated by fitting to a mixture of Gaussian functions with the 'normalmixEM()' function within the 'mixtools' library in R, version 4.2.3.[72] For eIF3 samples containing only 2 subunits, 2 initial guesses at 80 and 160 kDa were given as arguments. For eIF3 samples containing 3 or more subunits, 4 initial guesses at 80, 160, 290, and 365 kDa were given as arguments. This process was performed separately for three replicates of each solution mass distribution, and, for each distribution, the center of each peak was reported as the average and standard deviation across the three replicates.

Quantification of PIC binding and mRNA Recruitment Assays

The TIFF images obtained from the Amersham Typhoon 5 Biomolecular Imager (Cytiva, Catalog Number 29187191) for both PIC binding and mRNA recruitment assays were analyzed using ImageQuant TL, version 8.2.0.0 (Cytiva). For PIC binding assays, there are three bands corresponding to free mRNA, mRNA•PIC complexes, and mRNA•PIC•eIF3 complexes. Only the relative amount of mRNA•PIC and mRNA•PIC•eIF3 complexes are compared. A minimum profile background was subtracted from each lane in the gel and the mRNA•PIC•eIF3 complex fraction was calculated by dividing the intensity of the band corresponding to the mRNA•PIC•eIF3 complex by the total intensity of the lane (excluding the band corresponding to the free mRNA). For mRNA recruitment assays, a 'rubber band' background correction was applied, and the fraction of recruited mRNA was calculated by dividing the intensity of the band corresponding to the PIC by the total intensity of the lane.

Determination of Equilibrium Dissociation Constants

All binding data were fit to the quadratic binding equation:

$$A\left(\frac{(R+x+K)-\sqrt{(R+x+K)^2-(4Rx)}}{2R}\right)+0,$$

where A is the amplitude, R is the known concentration of the labeled component, K is the K_d^{app}, and O is the response offset.

To model the expected stoichiometry experiments in the titration regime at increasing mRNA concentrations for $eIF3_R$ and eIF3a, the experimentally measured mean K_d^{app}s were used to fix the K in the quadratic binding equation shown above with no offsets.

REFERENCES

1. Sokabe, M., and Fraser, C.S. (2019). Toward a Kinetic Understanding of Eukaryotic Translation. Cold Spring Harb Perspect Biol *11*. 10.1101/cshperspect.a032706.
2. Valášek, L.S. (2012). 'Ribozoomin' – Translation Initiation from the Perspective of the Ribosome-bound Eukaryotic Initiation Factors (eIFs). Curr Protein Pept Sci *13*, 305-330. 10.2174/138920312801619385.
3. Hinnebusch, A.G., and Lorsch, J.R. (2012). The mechanism of eukaryotic translation initiation: new insights and challenges. Cold Spring Harb Perspect Biol *4*. 10.1101/cshperspect.a011544.
4. Aitken, C.E., and Lorsch, J.R. (2012). A mechanistic overview of translation initiation in eukaryotes. Nature Structural & Molecular Biology *19*, 568-576. 10.1038/nsmb.2303.
5. Merrick, W.C., and Pavitt, G.D. (2018). Protein Synthesis Initiation in Eukaryotic Cells. Cold Spring Harb Perspect Biol *10*. 10.1101/cshperspect.a033092.
6. Valasek, L.S., Zeman, J., Wagner, S., Beznoskova, P., Pavlikova, Z., Mohammad, M.P., Hronova, V., Herrmannova, A., Hashem, Y., and Gunisova, S. (2017). Embraced by eIF3: structural and functional insights into the roles of eIF3 across the translation cycle. Nucleic Acids Res *45*, 10948-10968. 10.1093/nar/gkx805.
7. Wolf, D.A., Lin, Y., Duan, H., and Cheng, Y. (2020). eIF-Three to Tango: emerging functions of translation initiation factor eIF3 in protein synthesis and disease. J Mol Cell Biol *12*, 403-409. 10.1093/jmcb/mjaa018.
8. Hinnebusch, A.G. (2006). eIF3: a versatile scaffold for translation initiation complexes. Trends Biochem Sci *31*, 553-562. 10.1016/j.tibs.2006.08.005.
9. Cate, J.H. (2017). Human eIF3: from 'blobology' to biological insight. Philos Trans R Soc Lond B Biol Sci *372*. 10.1098/rstb.2016.0176.
10. Lin, Y., Li, F., Huang, L., Polte, C., Duan, H., Fang, J., Sun, L., Xing, X., Tian, G., Cheng, Y., et al. (2020). eIF3 Associates with 80S Ribosomes to Promote Translation Elongation, Mitochondrial Homeostasis, and Muscle Health. Mol Cell *79*, 575-587 e577. 10.1016/j.molcel.2020.06.003.
11. Beznoskova, P., Cuchalova, L., Wagner, S., Shoemaker, C.J., Gunisova, S., von der Haar, T., and Valasek, L.S. (2013). Translation initiation factors eIF3 and HCR1 control translation termination and stop codon read-through in yeast cells. PLoS Genet *9*, e1003962. 10.1371/journal.pgen.1003962.
12. Fujii, K., Zhulyn, O., Byeon, G.W., Genuth, N.R., Kerr, C.H., Walsh, E.M., and Barna, M. (2021). Controlling tissue patterning by translational regulation of signaling transcripts through the core translation factor eIF3c. Dev Cell *56*, 2928-2937 e2929. 10.1016/j.devcel.2021.10.009.
13. Meyer, K.D., Patil, D.P., Zhou, J., Zinoviev, A., Skabkin, M.A., Elemento, O., Pestova, T.V., Qian, S.B., and Jaffrey, S.R. (2015). 5' UTR m(6)A Promotes Cap-Independent Translation. Cell *163*, 999-1010. 10.1016/j.cell.2015.10.012.
14. Lee, A.S., Kranzusch, P.J., and Cate, J.H. (2015). eIF3 targets cell-proliferation messenger RNAs for translational activation or repression. Nature *522*, 111-114. 10.1038/nature14267.
15. Hayek, H., Eriani, G., and Allmang, C. (2022). eIF3 Interacts with Selenoprotein mRNAs. Biomolecules *12*. 10.3390/biom12091268.
16. Gonzalez-Sanchez, A.M., Castellanos-Silva, E.A., Diaz-Figueroa, G., and Cate, J.H.D. (2024). JUN mRNA translation regulation is mediated by multiple 5' UTR and start codon features. PLoS One *19*, e0299779. 10.1371/journal.pone.0299779.
17. Mestre-Fos, S., Ferguson, L., Trinidad, M., Ingolia, N.T., and Cate, J.H.D. (2023). eIF3 engages with 3'-UTR termini of highly translated mRNAs in neural progenitor cells. bioRxiv. 10.1101/2023.11.11.566681.

18. Hayek, H., Gross, L., Janvier, A., Schaeffer, L., Martin, F., Eriani, G., and Allmang, C. (2021). eIF3 interacts with histone H4 messenger RNA to regulate its translation. J Biol Chem *296*, 100578. 10.1016/j.jbc.2021.100578.
19. Hinnebusch, A.G. (2011). Molecular mechanism of scanning and start codon selection in eukaryotes. Microbiol Mol Biol Rev *75*, 434-467, first page of table of contents. 10.1128/MMBR.00008-11.
20. Llacer, J.L., Hussain, T., Dong, J., Villamayor, L., Gordiyenko, Y., and Hinnebusch, A.G. (2021). Large-scale movement of eIF3 domains during translation initiation modulate start codon selection. Nucleic Acids Res *49*, 11491-11511. 10.1093/nar/gkab908.
21. Llacer, J.L., Hussain, T., Saini, A.K., Nanda, J.S., Kaur, S., Gordiyenko, Y., Kumar, R., Hinnebusch, A.G., Lorsch, J.R., and Ramakrishnan, V. (2018). Translational initiation factor eIF5 replaces eIF1 on the 40S ribosomal subunit to promote start-codon recognition. Elife *7*. 10.7554/eLife.39273.
22. Aitken, C.E., Beznosková, P., Vlčkova, V., Chiu, W.-L., Zhou, F., Valášek, L.S., Hinnebusch, A.G., and Lorsch, J.R. (2016). Eukaryotic translation initiation factor 3 plays distinct roles at the mRNA entry and exit channels of the ribosomal preinitiation complex. eLife *5*, e20934. 10.7554/eLife.20934.
23. Mohammad, M.P., Munzarova Pondelickova, V., Zeman, J., Gunisova, S., and Valasek, L.S. (2017). In vivo evidence that eIF3 stays bound to ribosomes elongating and terminating on short upstream ORFs to promote reinitiation. Nucleic Acids Res *45*, 2658-2674. 10.1093/nar/gkx049.
24. Hronova, V., Mohammad, M.P., Wagner, S., Panek, J., Gunisova, S., Zeman, J., Poncova, K., and Valasek, L.S. (2017). Does eIF3 promote reinitiation after translation of short upstream ORFs also in mammalian cells? RNA Biol *14*, 1660-1667. 10.1080/15476286.2017.1353863.
25. Lee, A.S., Kranzusch, P.J., Doudna, J.A., and Cate, J.H. (2016). eIF3d is an mRNA cap-binding protein that is required for specialized translation initiation. Nature *536*, 96-99. 10.1038/nature18954.
26. Shah, M., Su, D., Scheliga, J.S., Pluskal, T., Boronat, S., Motamedchaboki, K., Campos, A.R., Qi, F., Hidalgo, E., Yanagida, M., and Wolf, D.A. (2016). A Transcript-Specific eIF3 Complex Mediates Global Translational Control of Energy Metabolism. Cell Rep *16*, 1891-1902. 10.1016/j.celrep.2016.07.006.
27. Armitage, J.P. (2024). Microbial Primer: The bacterial flagellum - how bacteria swim. Microbiology (Reading) *170*. 10.1099/mic.0.001406.
28. Brito Querido, J., Diaz-Lopez, I., and Ramakrishnan, V. (2024). The molecular basis of translation initiation and its regulation in eukaryotes. Nat Rev Mol Cell Biol *25*, 168-186. 10.1038/s41580-023-00624-9.
29. Will, C.L., and Luhrmann, R. (2011). Spliceosome structure and function. Cold Spring Harb Perspect Biol *3*. 10.1101/cshperspect.a003707.
30. Hoskins, A.A., Friedman, L.J., Gallagher, S.S., Crawford, D.J., Anderson, E.G., Wombacher, R., Ramirez, N., Cornish, V.W., Gelles, J., and Moore, M.J. (2011). Ordered and dynamic assembly of single spliceosomes. Science *331*, 1289-1295. 10.1126/science.1198830.
31. Wadhwa, N., Phillips, R., and Berg, H.C. (2019). Torque-dependent remodeling of the bacterial flagellar motor. Proc Natl Acad Sci U S A *116*, 11764-11769. 10.1073/pnas.1904577116.
32. Phan, L., Schoenfeld, L.W., Valasek, L., Nielsen, K.H., and Hinnebusch, A.G. (2001). A subcomplex of three eIF3 subunits binds eIF1 and eIF5 and stimulates ribosome binding of mRNA and tRNA(i)Met. EMBO J *20*, 2954-2965. 10.1093/emboj/20.11.2954.
33. Fraser, C.S., Lee, J.Y., Mayeur, G.L., Bushell, M., Doudna, J.A., and Hershey, J.W. (2004). The j-subunit of human translation initiation factor eIF3 is required for the stable binding of

eIF3 and its subcomplexes to 40 S ribosomal subunits in vitro. J Biol Chem *279*, 8946-8956. 10.1074/jbc.M312745200.
34. Herrmannova, A., Daujotyte, D., Yang, J.C., Cuchalova, L., Gorrec, F., Wagner, S., Danyi, I., Lukavsky, P.J., and Valasek, L.S. (2012). Structural analysis of an eIF3 subcomplex reveals conserved interactions required for a stable and proper translation pre-initiation complex assembly. Nucleic Acids Res *40*, 2294-2311. 10.1093/nar/gkr765.
35. Sun, C., Todorovic, A., Querol-Audi, J., Bai, Y., Villa, N., Snyder, M., Ashchyan, J., Lewis, C.S., Hartland, A., Gradia, S., et al. (2011). Functional reconstitution of human eukaryotic translation initiation factor 3 (eIF3). Proc Natl Acad Sci U S A *108*, 20473-20478. 10.1073/pnas.1116821108.
36. Mitchell, S.F., Walker, S.E., Algire, M.A., Park, E.-H., Hinnebusch, A.G., and Lorsch, J.R. (2010). The 5′-7-Methylguanosine Cap on Eukaryotic mRNAs Serves Both to Stimulate Canonical Translation Initiation and to Block an Alternative Pathway. Molecular Cell *39*, 950-962. 10.1016/j.molcel.2010.08.021.
37. Acker, M.G., Kolitz, S.E., Mitchell, S.F., Nanda, J.S., and Lorsch, J.R. (2007). Reconstitution of Yeast Translation Initiation. In Methods in Enzymology, J. Lorsch, ed. (Academic Press), pp. 111-145.
38. Liu, X., Schuessler, P.J., Sahoo, A., and Walker, S.E. (2019). Reconstitution and analyses of RNA interactions with eukaryotic translation initiation factors and ribosomal preinitiation complexes. Methods (San Diego, Calif.) *162-163*, 42-53. 10.1016/j.ymeth.2019.03.024.
39. Khoshnevis, S., Hauer, F., Milón, P., Stark, H., and Ficner, R. (2012). Novel insights into the architecture and protein interaction network of yeast eIF3. RNA (New York, N.Y.) *18*, 2306-2319. 10.1261/rna.032532.112.
40. Zeman, J., Itoh, Y., Kukačka, Z., Rosůlek, M., Kavan, D., Kouba, T., Jansen, M.E., Mohammad, M.P., Novák, P., and Valášek, L.S. (2019). Binding of eIF3 in complex with eIF5 and eIF1 to the 40S ribosomal subunit is accompanied by dramatic structural changes. Nucleic Acids Research *47*, 8282-8300. 10.1093/nar/gkz570.
41. Wu, D., and Piszczek, G. (2021). Standard protocol for mass photometry experiments. Eur Biophys J *50*, 403-409. 10.1007/s00249-021-01513-9.
42. Young, G., Hundt, N., Cole, D., Fineberg, A., Andrecka, J., Tyler, A., Olerinyova, A., Ansari, A., Marklund, E.G., Collier, M.P., et al. (2018). Quantitative mass imaging of single biological macromolecules. Science *360*, 423-427. 10.1126/science.aar5839.
43. Sonn-Segev, A., Belacic, K., Bodrug, T., Young, G., VanderLinden, R.T., Schulman, B.A., Schimpf, J., Friedrich, T., Dip, P.V., Schwartz, T.U., et al. (2020). Quantifying the heterogeneity of macromolecular machines by mass photometry. Nat Commun *11*, 1772. 10.1038/s41467-020-15642-w.
44. Gentry, R.C., Ide, N.A., Comunale, V.M., Hartwick, E.W., Kinz-Thompson, C.D., and Gonzalez, R.L., Jr. (2023). The mechanism of mRNA activation. bioRxiv. 10.1101/2023.11.15.567265.
45. Phan, L., Zhang, X., Asano, K., Anderson, J., Vornlocher, H.P., Greenberg, J.R., Qin, J., and Hinnebusch, A.G. (1998). Identification of a translation initiation factor 3 (eIF3) core complex, conserved in yeast and mammals, that interacts with eIF5. Mol Cell Biol *18*, 4935-4946. 10.1128/MCB.18.8.4935.
46. Valasek, L., Nielsen, K.H., and Hinnebusch, A.G. (2002). Direct eIF2-eIF3 contact in the multifactor complex is important for translation initiation in vivo. EMBO J *21*, 5886-5898. 10.1093/emboj/cdf563.
47. Valasek, L., Phan, L., Schoenfeld, L.W., Valaskova, V., and Hinnebusch, A.G. (2001). Related eIF3 subunits TIF32 and HCR1 interact with an RNA recognition motif in PRT1 required for eIF3 integrity and ribosome binding. EMBO J *20*, 891-904. 10.1093/emboj/20.4.891.
48. Llácer, Jose L., Hussain, T., Marler, L., Aitken, Colin E., Thakur, A., Lorsch, Jon R., Hinnebusch, Alan G., and Ramakrishnan, V. (2015). Conformational Differences between

Open and Closed States of the Eukaryotic Translation Initiation Complex. Molecular Cell *59*, 399-412. 10.1016/j.molcel.2015.06.033.
49. Querido, J.B., Sokabe, M., Kraatz, S., Gordiyenko, Y., Skehel, J.M., Fraser, C.S., and Ramakrishnan, V. (2020). Structure of a human 48S translational initiation complex. Science *369*, 1220-1227. 10.1126/science.aba4904.
50. Lapointe, C.P., Grosely, R., Sokabe, M., Alvarado, C., Wang, J., Montabana, E., Villa, N., Shin, B.S., Dever, T.E., Fraser, C.S., et al. (2022). eIF5B and eIF1A reorient initiator tRNA to allow ribosomal subunit joining. Nature *607*, 185-190. 10.1038/s41586-022-04858-z.
51. Dong, J., Aitken, C.E., Thakur, A., Shin, B.S., Lorsch, J.R., and Hinnebusch, A.G. (2017). Rps3/uS3 promotes mRNA binding at the 40S ribosome entry channel and stabilizes preinitiation complexes at start codons. Proc Natl Acad Sci U S A *114*, E2126-E2135. 10.1073/pnas.1620569114.
52. Yourik, P., Aitken, C.E., Zhou, F., Gupta, N., Hinnebusch, A.G., and Lorsch, J.R. (2017). Yeast eIF4A enhances recruitment of mRNAs regardless of their structural complexity. Elife *6*. 10.7554/eLife.31476.
53. Gupta, N., Lorsch, J.R., and Hinnebusch, A.G. (2018). Yeast Ded1 promotes 48S translation pre-initiation complex assembly in an mRNA-specific and eIF4F-dependent manner. Elife *7*. 10.7554/eLife.38892.
54. Jivotovskaya, A.V., Valasek, L., Hinnebusch, A.G., and Nielsen, K.H. (2006). Eukaryotic translation initiation factor 3 (eIF3) and eIF2 can promote mRNA binding to 40S subunits independently of eIF4G in yeast. Mol Cell Biol *26*, 1355-1372. 10.1128/MCB.26.4.1355-1372.2006.
55. Lamper, A.M., Fleming, R.H., Ladd, K.M., and Lee, A.S.Y. (2020). A phosphorylation-regulated eIF3d translation switch mediates cellular adaptation to metabolic stress. Science *370*, 853-856. 10.1126/science.abb0993.
56. Khoshnevis, S., Gunisova, S., Vlckova, V., Kouba, T., Neumann, P., Beznoskova, P., Ficner, R., and Valasek, L.S. (2014). Structural integrity of the PCI domain of eIF3a/TIF32 is required for mRNA recruitment to the 43S pre-initiation complexes. Nucleic Acids Res *42*, 4123-4139. 10.1093/nar/gkt1369.
57. Khoshnevis, S., Neumann, P., and Ficner, R. (2010). Crystal structure of the RNA recognition motif of yeast translation initiation factor eIF3b reveals differences to human eIF3b. PLoS One *5*. 10.1371/journal.pone.0012784.
58. ElAntak, L., Tzakos, A.G., Locker, N., and Lukavsky, P.J. (2007). Structure of eIF3b RNA recognition motif and its interaction with eIF3j: structural insights into the recruitment of eIF3b to the 40 S ribosomal subunit. J Biol Chem *282*, 8165-8174. 10.1074/jbc.M610860200.
59. Kouba, T., Rutkai, E., Karaskova, M., and Valasek, L. (2012). The eIF3c/NIP1 PCI domain interacts with RNA and RACK1/ASC1 and promotes assembly of translation preinitiation complexes. Nucleic Acids Res *40*, 2683-2699. 10.1093/nar/gkr1083.
60. Hanachi, P., Hershey, J.W., and Vornlocher, H.P. (1999). Characterization of the p33 subunit of eukaryotic translation initiation factor-3 from Saccharomyces cerevisiae. J Biol Chem *274*, 8546-8553. 10.1074/jbc.274.13.8546.
61. Jarmoskaite, I., AlSadhan, I., Vaidyanathan, P.P., and Herschlag, D. (2020). How to measure and evaluate binding affinities. Elife *9*. 10.7554/eLife.57264.
62. Fei, J., Kosuri, P., MacDougall, D.D., and Gonzalez, R.L. (2008). Coupling of Ribosomal L1 Stalk and tRNA Dynamics during Translation Elongation. Molecular Cell *30*, 348-359. 10.1016/j.molcel.2008.03.012.
63. Blanchard, S.C., Kim, H.D., Gonzalez, R.L., Jr., Puglisi, J.D., and Chu, S. (2004). tRNA dynamics on the ribosome during translation. Proc Natl Acad Sci U S A *101*, 12893-12898. 10.1073/pnas.0403884101.
64. Blanchard, S.C., Gonzalez, R.L., Kim, H.D., Chu, S., and Puglisi, J.D. (2004). tRNA selection and kinetic proofreading in translation. Nat Struct Mol Biol *11*, 1008-1014. 10.1038/nsmb831.

65. Erzberger, J.P., Stengel, F., Pellarin, R., Zhang, S., Schaefer, T., Aylett, C.H.S., Cimermancic, P., Boehringer, D., Sali, A., Aebersold, R., and Ban, N. (2014). Molecular Architecture of the 40S·eIF1·eIF3 Translation Initiation Complex. Cell *159*, 1227-1228. 10.1016/j.cell.2014.11.001.
66. Simonetti, A., Brito Querido, J., Myasnikov, A.G., Mancera-Martinez, E., Renaud, A., Kuhn, L., and Hashem, Y. (2016). eIF3 Peripheral Subunits Rearrangement after mRNA Binding and Start-Codon Recognition. Mol Cell *63*, 206-217. 10.1016/j.molcel.2016.05.033.
67. Simonetti, A., Guca, E., Bochler, A., Kuhn, L., and Hashem, Y. (2020). Structural Insights into the Mammalian Late-Stage Initiation Complexes. Cell Reports *31*, 107497. 10.1016/j.celrep.2020.03.061.
68. Pavitt, G.D., Ramaiah, K.V., Kimball, S.R., and Hinnebusch, A.G. (1998). eIF2 independently binds two distinct eIF2B subcomplexes that catalyze and regulate guanine-nucleotide exchange. Genes Dev *12*, 514-526. 10.1101/gad.12.4.514.
69. Costa, S.J., Coelho, E., Franco, L., Almeida, A., Castro, A., and Domingues, L. (2013). The Fh8 tag: a fusion partner for simple and cost-effective protein purification in Escherichia coli. Protein Expr Purif *92*, 163-170. 10.1016/j.pep.2013.09.013.
70. Walker, S.E., and Fredrick, K. (2008). Preparation and evaluation of acylated tRNAs. Methods *44*, 81-86. 10.1016/j.ymeth.2007.09.003.
71. Venables, W.N., Ripley, B.D., and Venables, W.N. (2002). Modern applied statistics with S, 4th Edition (Springer).
72. Benaglia T, C.D., Hunter DR, Young D (2009). mixtools: An R Package for Analyzing Finite Mixture Models. Journal of Statistical Software *32(6)*, 1–29.

SUPPLEMENTAL FIGURES

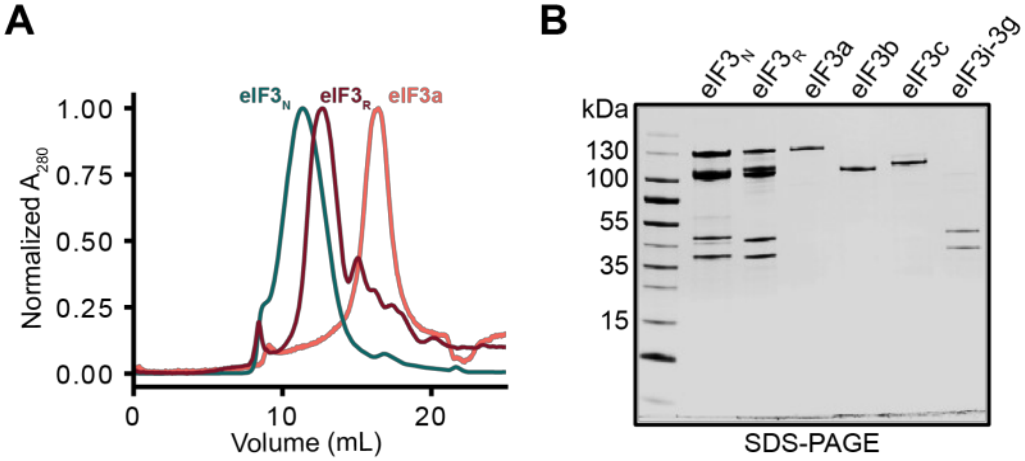

Supplemental Figure 1. Preparation of eIF3$_N$ and eIF3$_R$ (A) Size-exclusion chromatograms for eIF3$_N$, eIF3$_R$, and eIF3a. **(B)** SDS-PAGE gel showing eIF3$_N$, eIF3$_R$, and each recombinant eIF3 subunit.

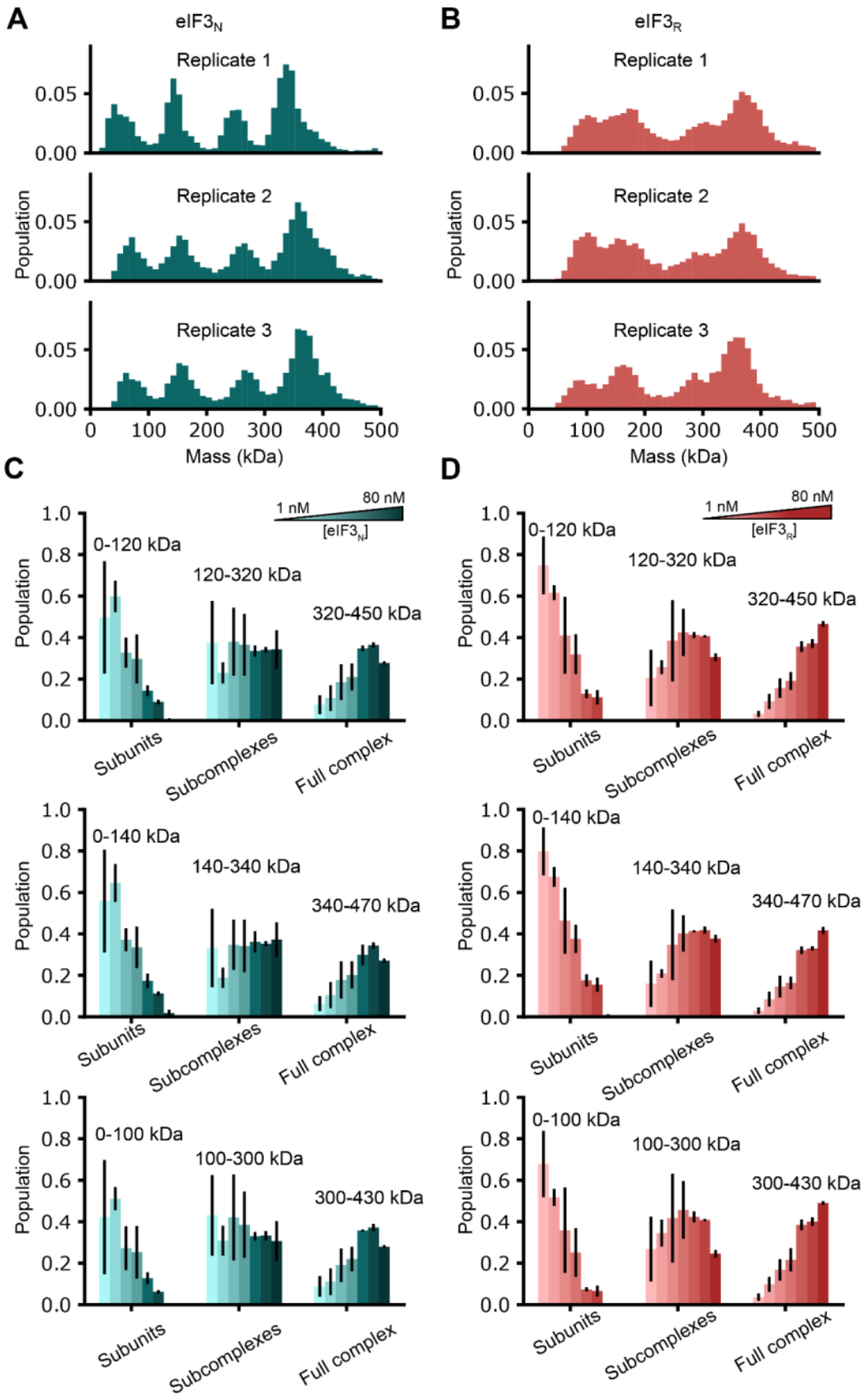
A
eIF3N
Replicate 1
Replicate 2
Replicate 3
Population
0.05
0.00
0
100
200
300
400
500
Mass (kDa)
B
eIF3R
C
1 nM
80 nM
[eIF3N]
0-120 kDa
120-320 kDa
320-450 kDa
0-140 kDa
140-340 kDa
340-470 kDa
0-100 kDa
100-300 kDa
300-430 kDa
Subunits
Subcomplexes
Full complex
D
[eIF3R]

Supplemental Figure 2. Mass photometry of eIF3$_N$ and eIF3$_R$, related to Figure 1. (A) Individual replicates shown separately for experiments depicted in Figure 1A. **(B)** Individual replicates shown separately for experiments depicted in Figure 1B. **(C)** Bar graph showing the change in populations of subunits, subcomplexes, and the full complex as a function of concentration for eIF3$_N$ using the threshold cutoffs depicted in Figure 1C and upon shifting those threshold cutoffs (middle and bottom). The bars represent the average of the population, and the error bars represent the standard deviation of the population across three replicates. **(D)** The equivalent plots as shown in (C) for eIF3$_R$.

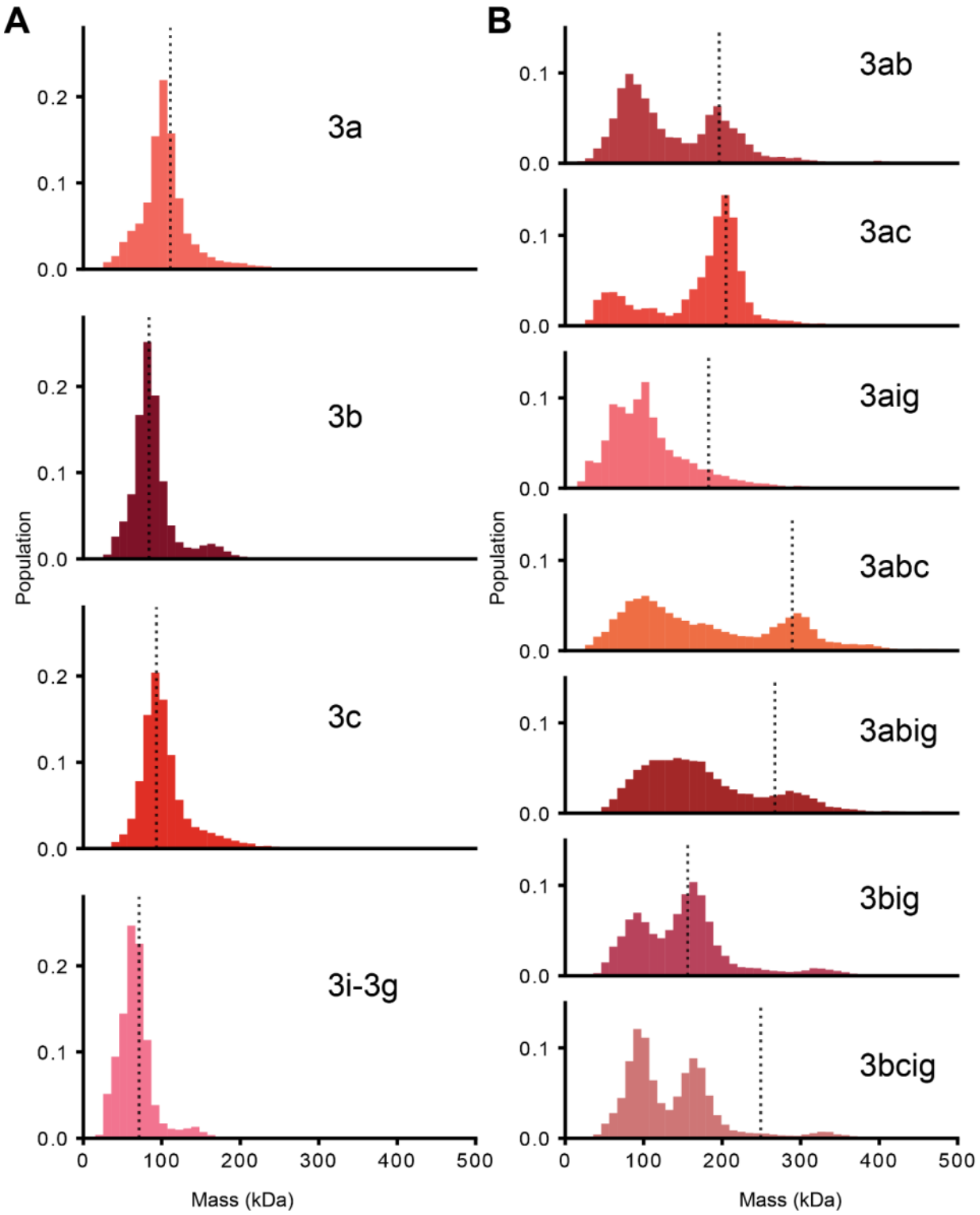

Supplemental Figure 3. Identification of eIF3-subcomplexes using mass photometry (A) Histograms of three combined replicates for each indicated recombinant eIF3 subunit. **(B)**

Histograms of three combined replicates for each indicated eIF3 subcomplex. The dotted black line indicates the sequence-determined molecular mass for the eIF3 species.

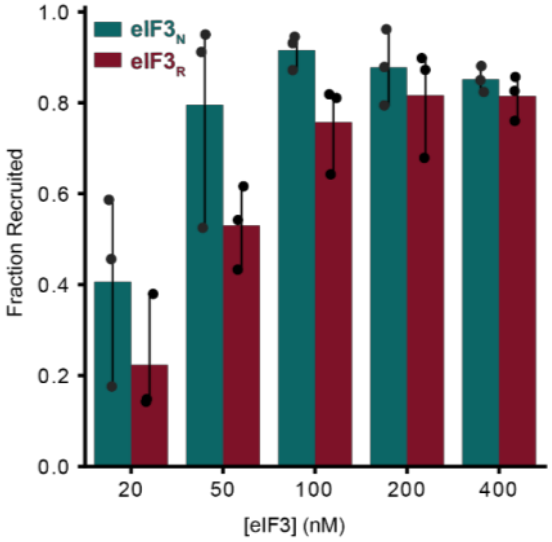

Supplemental Figure 4. Cap-dependent mRNA recruitment by eIF3$_N$ and eIF3$_R$. Extent of mRNA recruitment at various concentrations of eIF3$_N$ and eIF3$_R$.

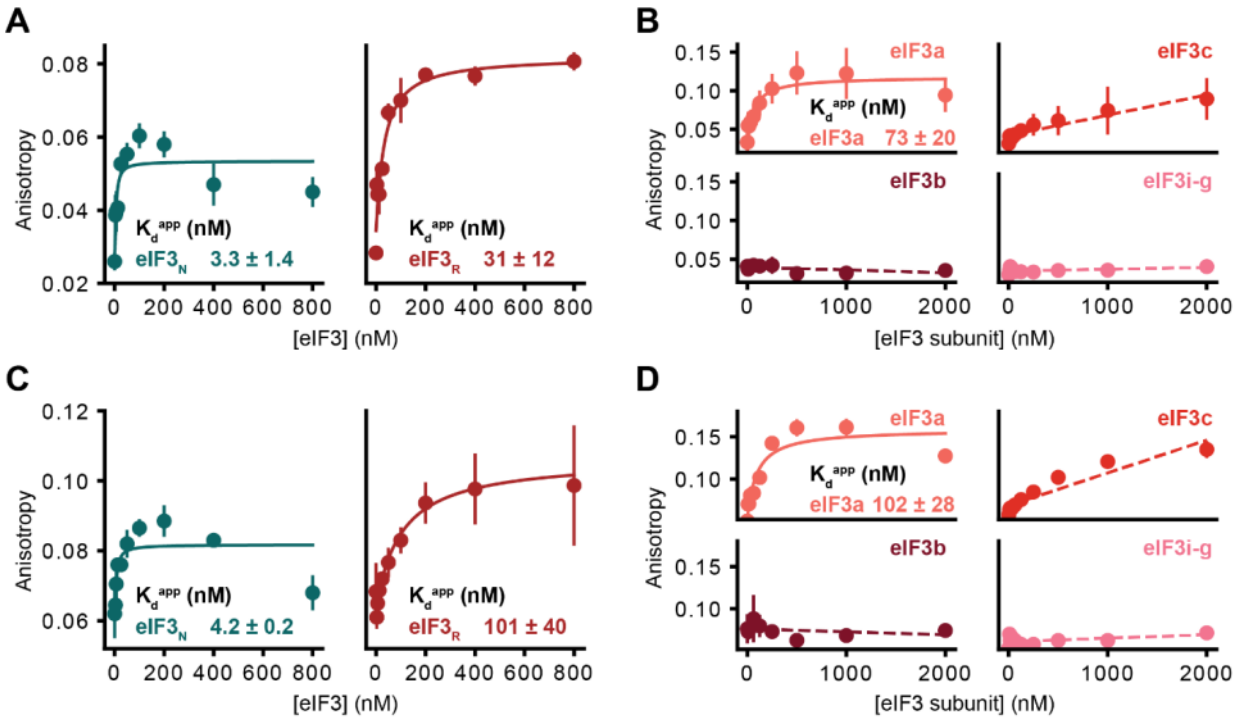

Supplemental Figure 5. $eIF3_N$, $eIF3_R$, and eIF3 subunits binding to two additional mRNAs. **(A)** Fluorescence-anisotropy RNA binding experiments comparing $eIF3_N$ and $eIF3_R$ binding to a model mRNA composed largely of a repetitive UC sequence ('polyUC') **(B)** The same experiments as (A) for individual eIF3 subunits **(C)** Fluorescence-anisotropy RNA binding experiments comparing $eIF3_N$ and $eIF3_R$ binding to the first 51 nucleotides of the rpl41a mRNA ('natural') **(D)** The same experiments as (C) for individual eIF3 subunits

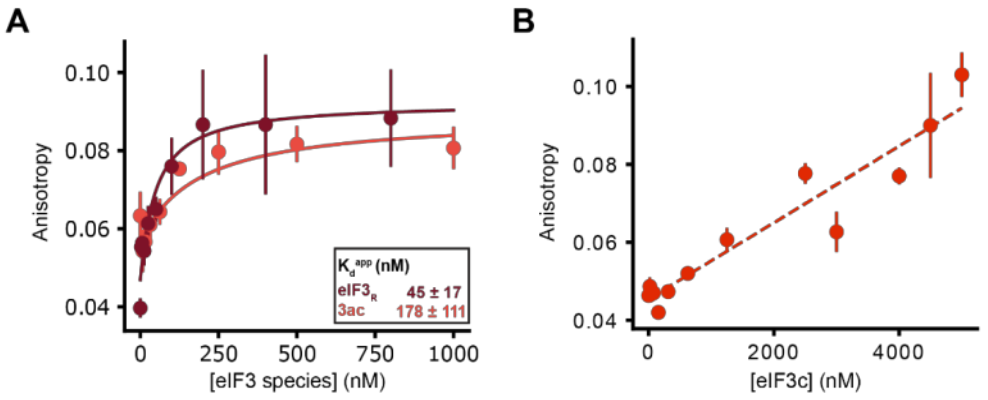

Supplemental Figure 6. eIF3ac binds mRNA nearly identically to $eIF3_R$ and an extended eIF3c titration does not saturate the mRNA (A) Fluorescence-anisotropy binding experiment comparing $eIF3_R$ and eIF3ac. **(B)** Fluorescence anisotropy binding experiment titrating up to 5000 nM eIF3c.

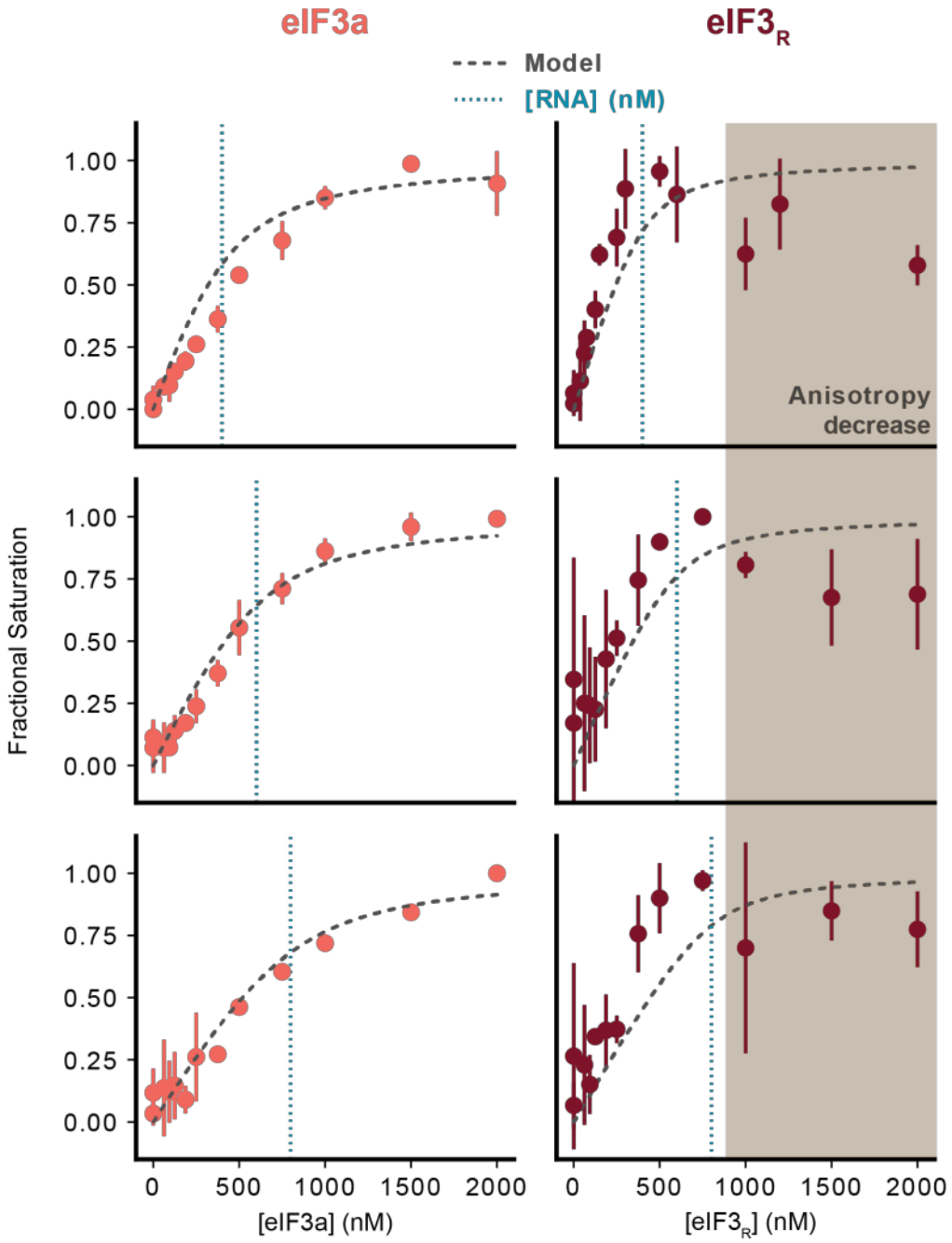

Supplemental Figure 7. Fluorescence anisotropy binding experiments increasing the total concentration of mRNA (i.e. in the 'titration-regime'). (A) Fluorescence-anisotropy RNA binding experiments of eIF3a to the polyCAA mRNA sequence with increasing [mRNA]: 400 nM (top), 600 nM (middle), and 800 nM (bottom) compared to a model protein-RNA binding interaction with a K_d of 119 nM (Figure 3A). Normalized anisotropy is shown to compare experimental data to the modeled curves **(B)** The same experiments as in (A) for $eIF3_R$ (using a K_d of 45 nM for the model, Figure 3A).

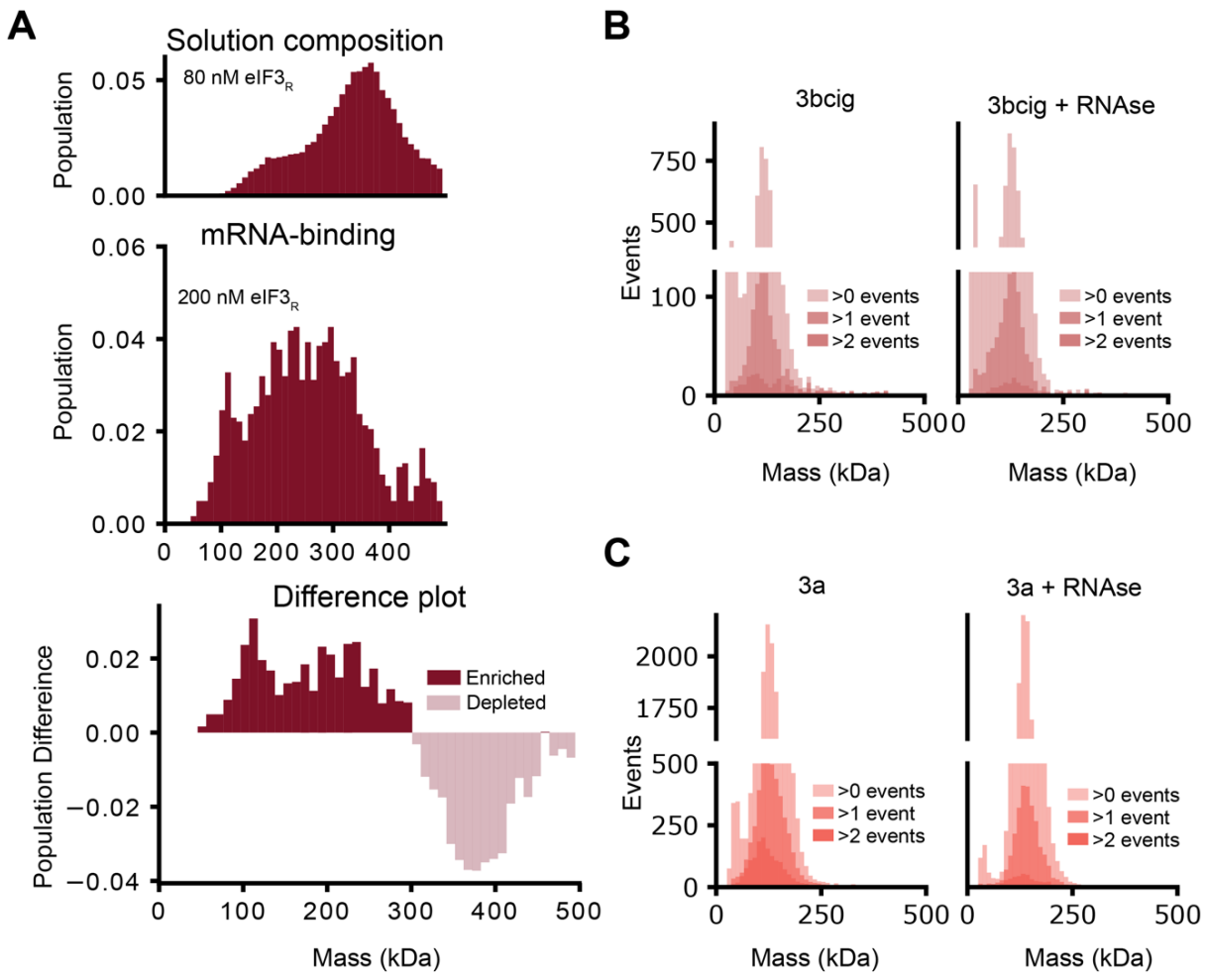

Supplemental Figure 8. eIF3a-containing subcomplexes are over-represented in mRNA-binding relative to their solution distribution. (A) The solution composition of 80 nM $eIF3_R$ determined using standard mass photometry on underivatized coverslips is shown above the mRNA-binding mass distribution of 200 nM $eIF3_R$. The bottom graph is the difference plot of the solution distribution of 80 nM $eIF3_R$ subtracted from the mRNA-binding distribution, highlighting that while the full complex is likely most abundant at 200 nM, subcomplexes are over-represented in mRNA-binding. **(B)** mRNA-binding mass distributions of an eIF3a dropout mixture. Upon filtering for repetitive events at individual pixels (left) and upon addition of RNAse (right). **(C)** The equivalent plots as shown in (B) for eIF3a alone.

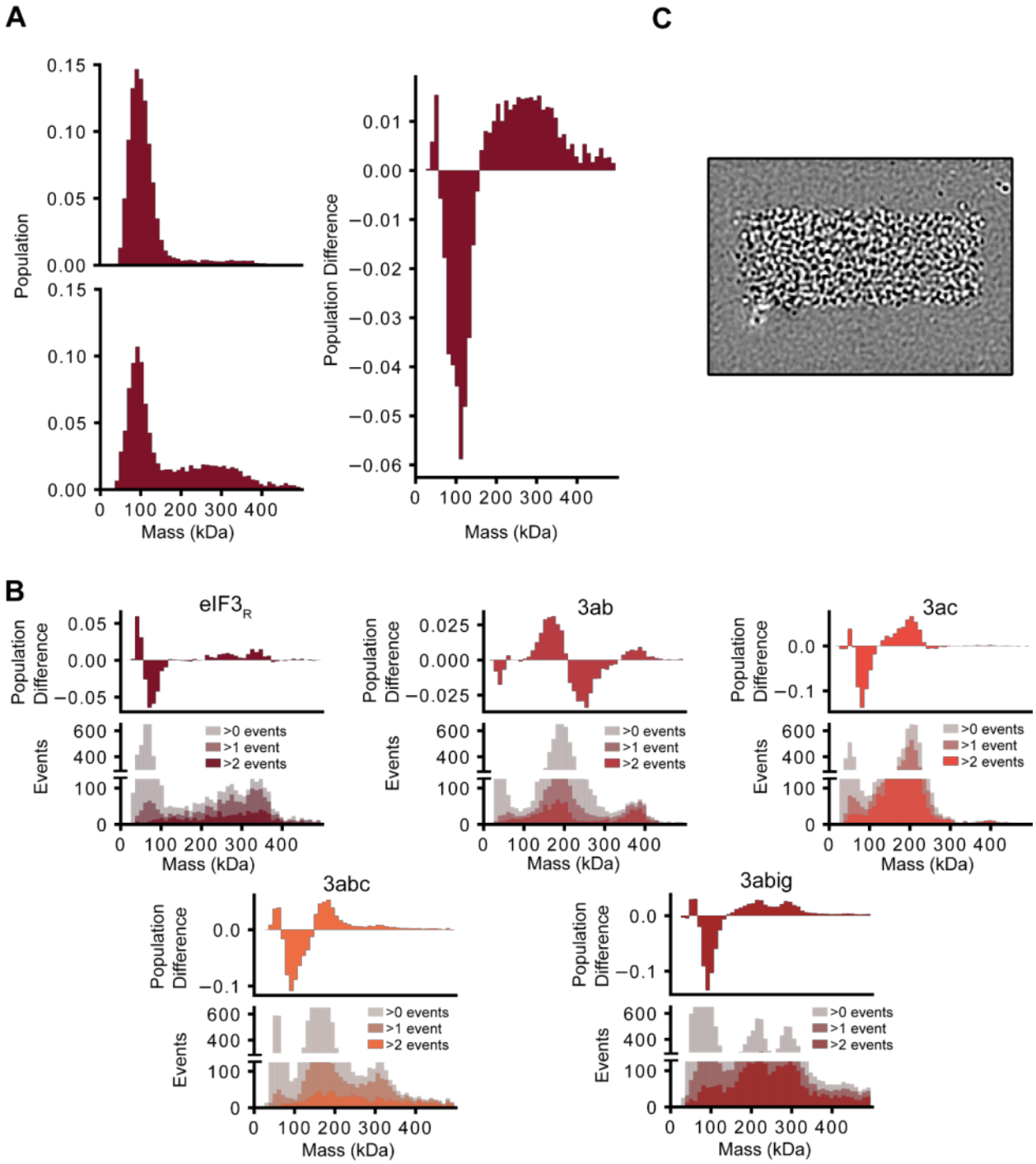

Supplemental Figure 9. The addition of RNAse highlights which part of the mass distribution makes specific mRNA interactions. (A) The mRNA-binding mass distributions of 200 nM $eIF3_R$ before (bottom) and after (top) addition of RNAse. Left is the population difference plot generated by subtracting the mass distribution after addition of RNAse from the mass distribution before addition of RNAse. **(B)** The same difference plots as in (A) but for 30 nM of each indicated subcomplex. **(C)** An example frame after laser-induced heating of an mRNA-binding experiment with 30 nM $eIF3_R$. A 'small' field of view was imaged for ~ 2 minutes, then the field of view was changed to 'large' and this image was captured.

Supplemental Table 1. Molecular Masses of eIF3 species. Each value is the average of three replicates and the error is the standard deviation across those replicates.

Molecular Masses from Mass Photometry (kDa)

	Species 1	Species 2	Species 3	Species 4	Predicted mass
$eIF3_N$	70 ± 8	158 ± 5	261 ± 8	368 ± 12	360.5
$eIF3_R$	97 ± 3	170 ± 2	275 ± 11	367 ± 8	360.5
3abc	92 ± 18	172 ± 6	271 ± 31	321 ± 23	289
3abig	101 ± 5	159 ± 6	280 ± 17	397 ± 69	267.3
3ab	89 ± 11	193 ± 5	–	–	195.8
3ac	65 ± 5	201 ± 4	–	–	204.7
3aig	106 ± 24	193 ± 22	–	–	183
3big	95 ± 3	167 ± 1	275 ± 41	310 ± 43	155.8
3a	110 ± 12	–	–	–	111.5
3b	96 ± 5	–	–	–	84.3
3c	111 ± 6	–	–	–	93.2
3ig	74 ± 4	–	–	–	(39.8) and (31.7)

Supplemental Table 2. Summary of K_d^{app} values. Each value is the average of three replicates and the error is the standard deviation across those replicates.

Summary of K_d^{app}'s (nM)

	polyCAA (50nt)	45 nt	40 nt	polyUC	rpl41a
$eIF3_N$[a]	4.1 ± 1.3	8.3 ± 2.7	N.D.	3.3 ± 1.4	4.2 ± 0.2
$eIF3_R$[a]	47 ± 18	5.8 ± 0.7	N.D.	31 ± 12	101 ± 40
eIF3a	116 ± 55	45 ± 4.2	N.D.	73 ± 20	102 ± 28
eIF3b	N.D.	–	–	N.D.	N.D.
eIF3c	1226 ± 721	–	–	N.D.[b]	1214 ± 807
eIF3i-3g	N.D.	–	–	N.D.	N.D.

[a] K_d^{app} assuming two-component, single-site binding
[b] General anisotropy increase but unable to fit
N.D. Not Determined/unable to fit
– Experiment not performed